AD-A128 333 THE DEVELOPMENT AND EVALUATION OF POINT DEFECT MODELS 1/1
FOR THE GROWTH OF P..(U) OHIO STATE UNIV COLUMBUS
FONTANA CORROSION CENTER R LIANG ET AL. 28 FEB 83
UNCLASSIFIED FCC-4445-2 N00014-82-K-0265 F/G 11/6 NL

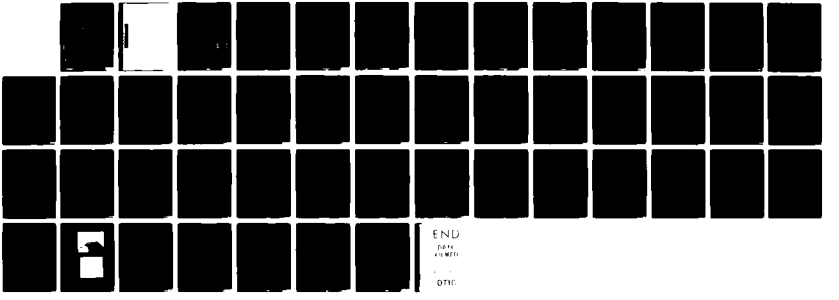

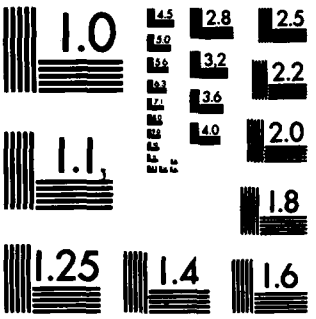

MICROCOPY RESOLUTION TEST CHART
NATIONAL BUREAU OF STANDARDS-1963-A

AD A128333

ONR N00014-82-K-0265

RF 714445

FCC 4445-2

Annual Report

March 1, 1982 through February 28, 1983

THE DEVELOPMENT AND EVALUATION OF POINT DEFECT MODELS FOR THE GROWTH OF PASSIVE FILMS ON SINGLE CRYSTAL, POLYCRYSTALLINE, AND AMORPHOUS METAL SURFACES.

DTIC
ELECTE
MAY 1 9 1983
A

Ru-Yu Liang
Kuan-Shaur Lei
B.G. Pound
D.D. Macdonald, Principal Investigator

This document has been approved for public release and sale; its distribution is unlimited.

TABLE OF CONTENTS

Accession For
NTIS GRA&I
DTIC TAB
Unannounced
Justification
By
Distribution/
Availability Codes
Dist Avail and/or Special
A

LIST OF FIGURES

LIST OF TABLES

EXECUTIVE SUMMARY

This research program was undertaken to provide data with which to test the validity of the point defect model developed by Macdonald and co-workers to describe the growth and breakdown of films on metals. The study is comprised of two tasks. Task 1 is an investigation of the growth of passive films on nickel and iron in phosphate solutions whereas Task 2 is concerned with the film breakdown behavior on single crystal and polycrystalline metals (Ni, Fe) and alloys (Fe-Ni, Fe-Ni-Cr) in borate buffer solutions with chloride present.

Task 1: Film Growth

The growth of hydroxide films on single crystal nickel has been investigated using ac impedance and ellipsometric techniques. The impedance data plotted in the complex plane show similar features over a pH range of 7 to 12. Typically, the complex plane diagrams for potentials less than 0.5V (SCE) exhibit a well-defined semi-circle at high frequencies and linear Warburg (diffusion)-type behavior at low frequencies. At potentials above 0.5V, the low frequency data deviate from the Warburg line. This change in the impedance loci was shown from cyclic voltammetry to be associated with the conversion of $Ni(OH)_2$ to NiOOH at approximately 0.5V.

The theory for film growth based on the point defect model predicts firstly that the product of the Warburg coefficient σ, and the dc current, I_{dc} should be a constant, and secondly that σ should be independent of film thickness. Data for $I_{dc} \cdot \sigma$ for $E<0.5V$ were indeed found to be constant within experimental error at pH values of 9 and 11. In addition, σ was generally found to be independent of film thickness.

It was found that sufficient time is required for the rate of film growth to become small enough such that the thickness of the film and therefore I_{dc} do not change significantly over the duration of a set of impedance measurements. However, while the film can then be considered to be in a "steady state", the value of I_{dc} may well differ significantly from the dc current at

a substantially longer time. Indeed, the lack of a constant $I_{dc}\cdot\sigma$ product at pH values other than 9 and 11 can be largely attributed to the difficulty in measuring accurately the small dc currents (<1μA), and particularly in determining a more satisfactory state. Nevertheless, the constancy of $I_{dc}\cdot\sigma$ shown for two values of pH indicates considerable promise for the point defect model.

Task 2: Film Breakdown

The breakdown of hydroxide films on single crystal nickel is under examination using electrochemical and metallurgical techniques. The first priority was to obtain a reproducible, defect-free sample surface since initial film breakdown experiments had given inconsistent results due to surface defects that remained after mechanical polishing. Several combinations of mechanical, chemical and electrolytic polishing procedures were tested. Optical micrographs showed that a mechanical polish down to 0.05μm following by electropolishing in 57% H_2SO_4 gave the most satisfactory surface condition.

The use of a sealant and a Teflon shield around the metal sample was found to be necessary to avoid crevice corrosion at the metal/holder junction. The shield was designed to allow unrestricted access for the electrolyte but was demonstrated to be effective in preventing any crevice corrosion.

Several film breakdown experiments have been performed on β-$Ni(OH)_2$ films formed on electropolished nickel samples at different chloride concentrations, passivation times and anodic sweep rates. Film breakdown potentials were determined from current/potential sweep curves and were shown to become more anodic as either the sweep rate or the passivation time increases; a higher sweep rate allows less time for pit initiation following the critical breakdown potential whereas a longer passivation time simply permits a thicker film to form. A decrease in the chloride ion concentration also causes an anodic shift in the breakdown potential but at sufficiently low Cl^- concentrations and/or thick films, no film breakdowns were detected. Instead, the current exhibited a maximum on both the anodic and the cathodic sweep, as noted in the first period of this study. These maxima corresponded to the oxidation of β-$Ni(OH)_2$ to β-NiOOH and the conjugate reduction reaction respectively.

Data for the film breakdown potentials as a function of sweep rate will allow the critical breakdown potentials, V_c to be obtained. The theory based on the point defect model predicts that V_c should be proportional to -log (activity of Cl^-) and therefore values of V_c obtained from the experimental data can be used directly to examine the validity of the point defect model.

Task 1

IMPEDANCE STUDY OF THE GROWTH OF PASSIVE FILMS ON Ni SINGLE CRYSTAL IN PHOSPHATE SOLUTIONS

Ru-Yu Liang, Bruce Pound, and Digby D. Macdonald

GENERAL OBJECTIVE

The point defect model for film growth developed by Lin, Chao, and Macdonald[1] has shown considerable agreement with the observed film growth behavior of iron in borate buffer solutions. However, the limited data for the iron-borate system seems insufficient to test the generality of this model.

The purpose of this study, therefore, is to obtain more data from other systems in order to assess the general applicability of the point defect model. In this study, the film growth behavior of nickel in phosphate solutions was investigated using the AC impedance and ellipsometric techniques.

EXPERIMENTAL

The experimental setup, which is represented schematically in Figure 1, is composed of four main parts:

(1) a Solartron Model 1172 Frequency Response analyzer (FRA) which is able to determine the impedance of metal/water systems as a function of frequency of the AC potential perturbation which is superimposed on a DC applied potential. In order to avoid a high noise-to-signal ratio at low frequencies, an AC potential of 0.02 volt instead of the commonly used 0.01 volt was employed. In addition, a resistor with a very large resistance, i.e. 10 kΩ, was used for the same purpose,

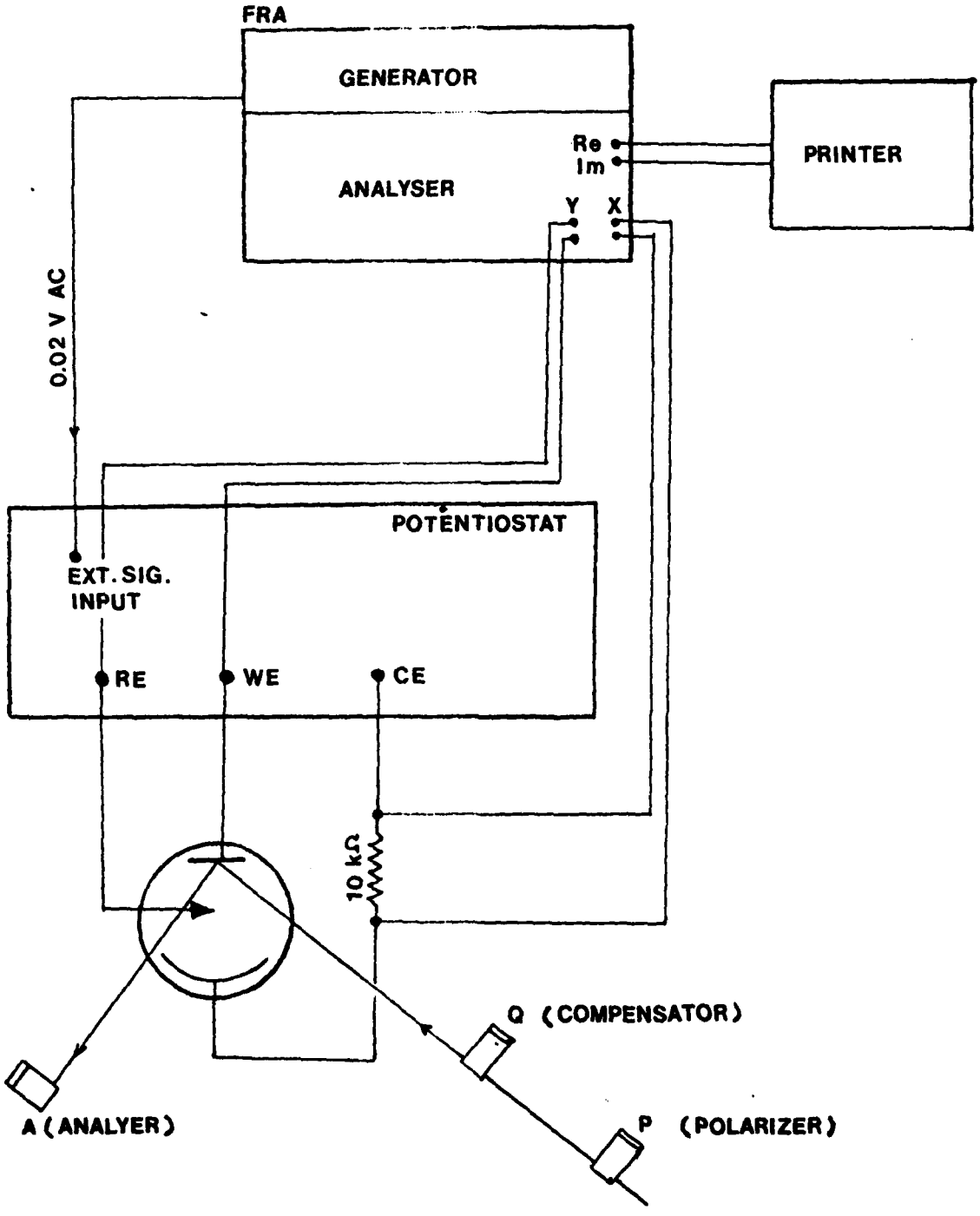

Figure 1. Schematic diagram of experimental setup for the measurements of AC impedances and ellipsometric data.

(2) a potentiostat (Model PAR 173) which supplies a constant potential difference between a working electrode and a reference electrode,

(3) an electrochemical cell which contains a working electrode (Ni specimen), a counter electrode (Pt net) and a reference electrode (non-polarizable saturated calomel electrode, SCE), and

(4) a manual ellipsometer which is able to measure two ellipsometric parameters, A and P, from which the film thickness can be calculated using a computer program.

In this study, a nickel single crystal with an exposed surface orientation (111) was immersed in deaerated 0.1N sodium phosphate solutions ranging in pH from 7 to 12. For each pH, three to five potentials in the passive region, i.e. +100 mV_{SCE} to +700 mV_{SCE}, were selected for investigation. The potential was stepped anodically to a new value after measurement of both the AC impedance and ellipsometric parameters without removing the specimen from the electrochemical cell and repolishing it. The two polarization curves at pH=7 and pH=8 shown in Figure 2 were obtained to ensure that the selected potentials were in the passive region.

RESULTS AND DISCUSSIONS

According to the point defect model, the film thickness is expected to change with log (time) and the transient current density should vary inversely with time for thick films. Consequently, a true steady state is unlikely to be achieved in such a situation. Table 1 shows how the "steady state" was defined for the current work. For each applied potential, sufficient time for the dc polarization, e.g., 12 hr at 100 mV, was allowed so that there was

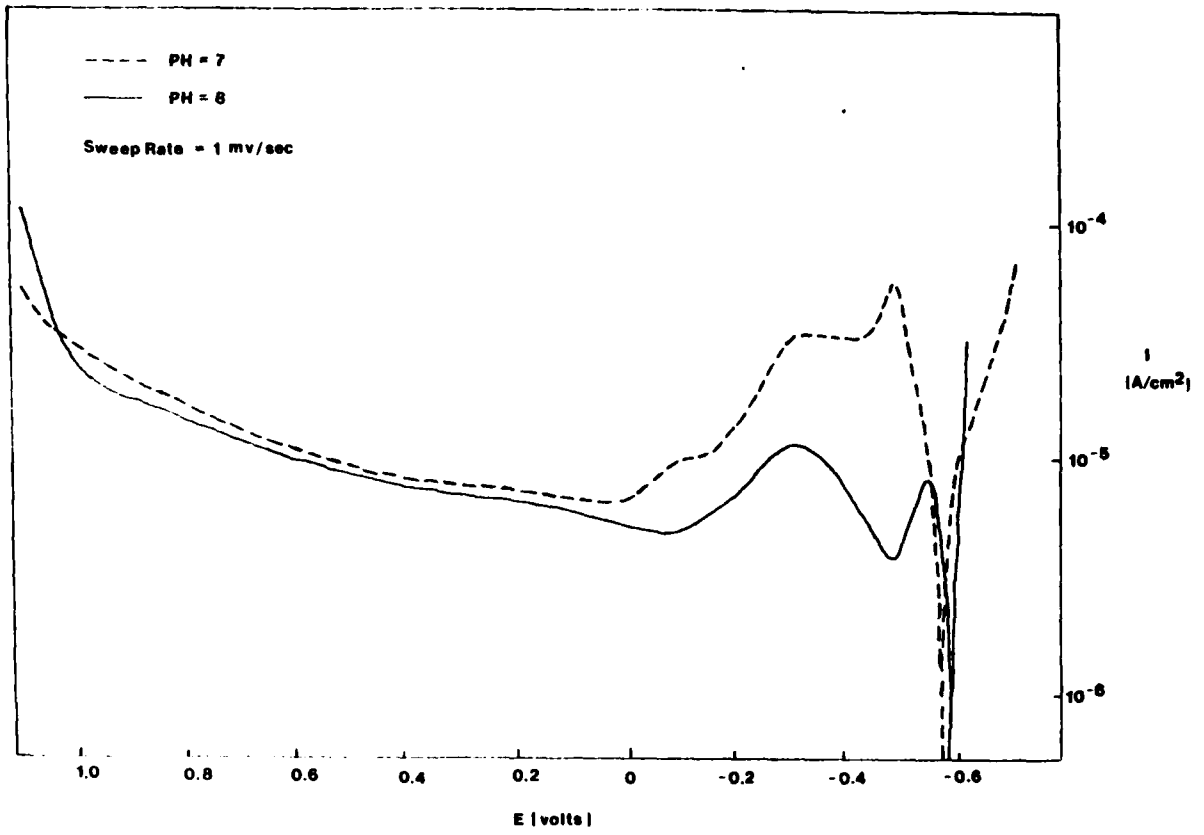

Figure 2. Polarization curve of Ni (111) in 0.1N phosphate solutions (pH = 7 and pH = 8).

negligible difference between the two sets of ellipsometric parameters, one set being measured before and the other after the AC impedance measurements. Therefore, during the AC impedance measurements at each potential, the film thickness and also i_{dc} changed insignificantly and the passive film was then considered to be in a steady state.

Table 1

THE DATA OBTAINED AT THE "STEADY STATE" OF FILM GROWTH ON Ni(111) IN PHOSPHATE SOLUTION (pH=11)

E/mV	P	A	I_{dc} μA
-1,000 (Bare Surface)	88.49	31.81	
+100	90.50	33.14 (12 hrs)*	0.4
	90.46	33.16 (1.5 hrs for AC imped.)	0.4
+200	90.98	33.35 (5 hrs)*	0.6
	90.99	33.37 (1.5 hrs.)	0.6
+300	91.08	33.97 (10 hrs)*	0.5
	91.29	34.07 (1.5 hrs)	0.5
+400	91.26	34.28 (5 hrs)*	0.6
	91.36	34.27 (1.5 hrs)	0.5
+500	92.06	34.43 (4 hrs.)*	0.7
	91.90	34.58 (1.5 hrs.)	0.8

* Time at each potential prior to commencement of impedance measurements.

Figures 3 to 8 show the complex impedance plane plots for passive nickel (111) in 0.1N phosphate solutions for various values of pH. At potentials less positive than +500 mV_{SCE}, the complex impedances show the Warburg-type response where the data points obtained at those potentials fall on the 45° line. However, the impedances at the potentials more positive than +500 mV_{SCE} do not show the Warburg form. They deviate from the 45° line as the frequency decreases. The impedance locus at 500 mV exhibits either type of behavior depending on the pH. This change in the impedance pattern is due to the conversion[2] of $Ni(OH)_2$ to NiOOH. Evidence of this conversion was obtained from two experiments. Firstly in a triangular potential sweep test (Figure 9) on Ni in a phosphate solution (pH=12) the current density increases abruptly at +500 mV_{SCE}. This increase is associated with the oxidation of $Ni(OH)_2$.

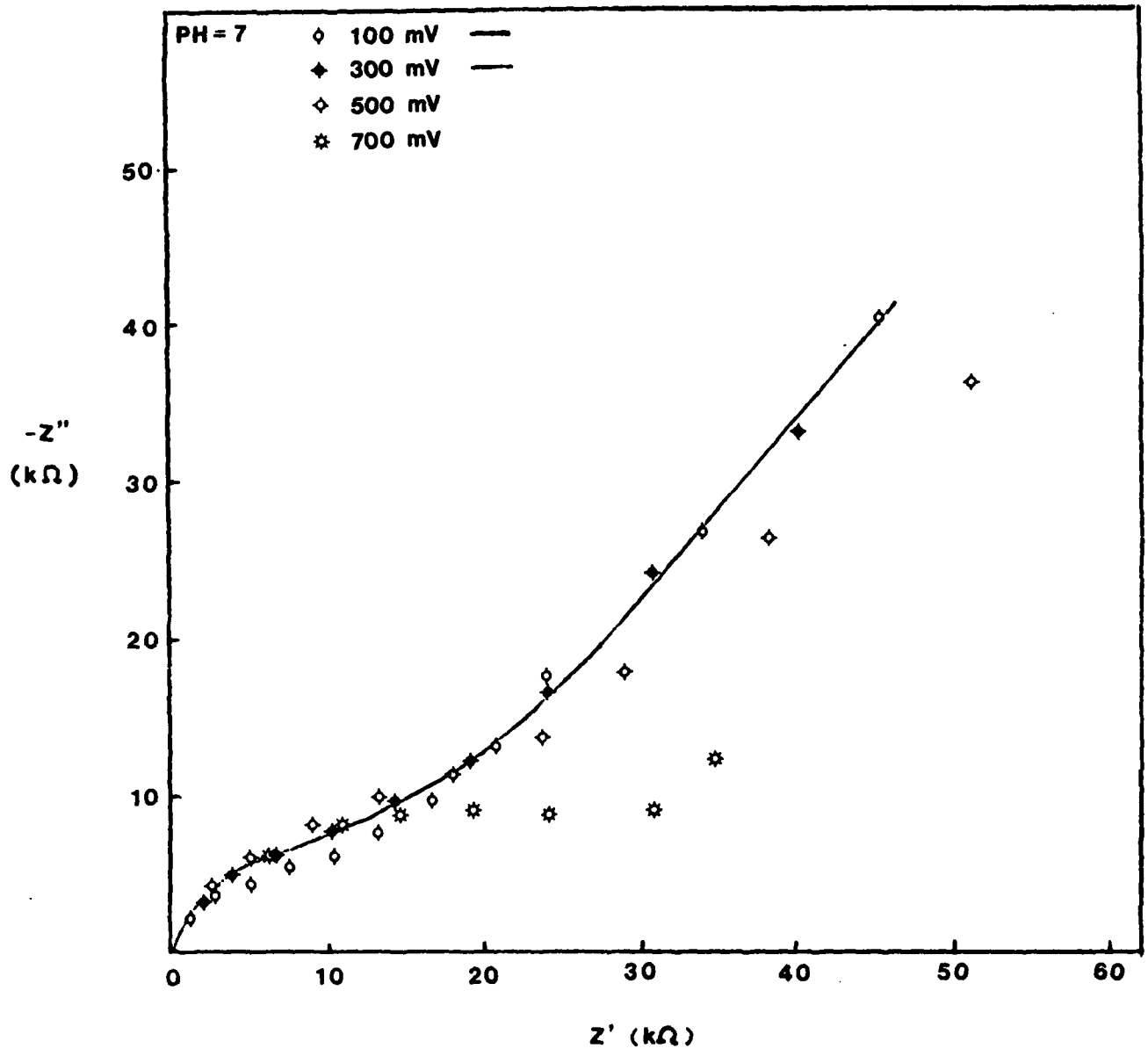

Figure 3. Complex impedance plane for passive nickel (111) in 0.1N phosphate solution (pH = 7).

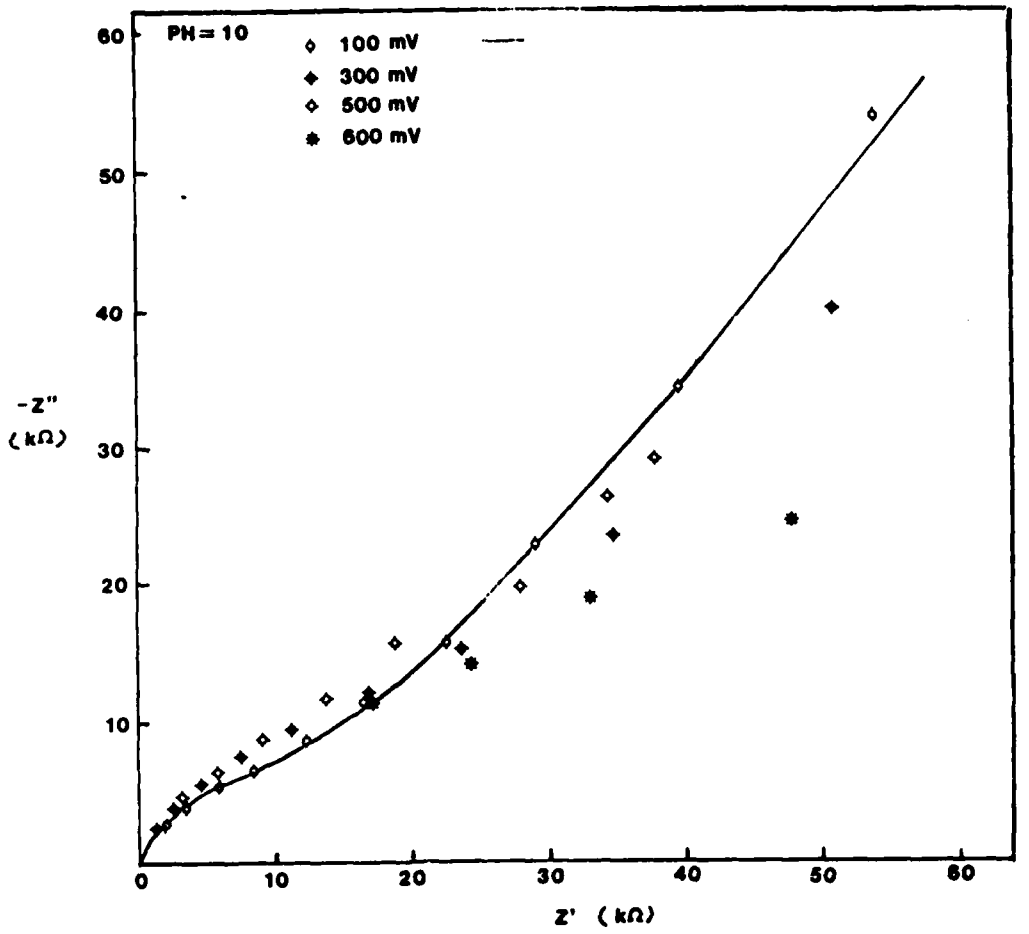

Figure 4. Complex impedance plane for passive nickel (111) in 0.1N phosphate solution (pH = 8).

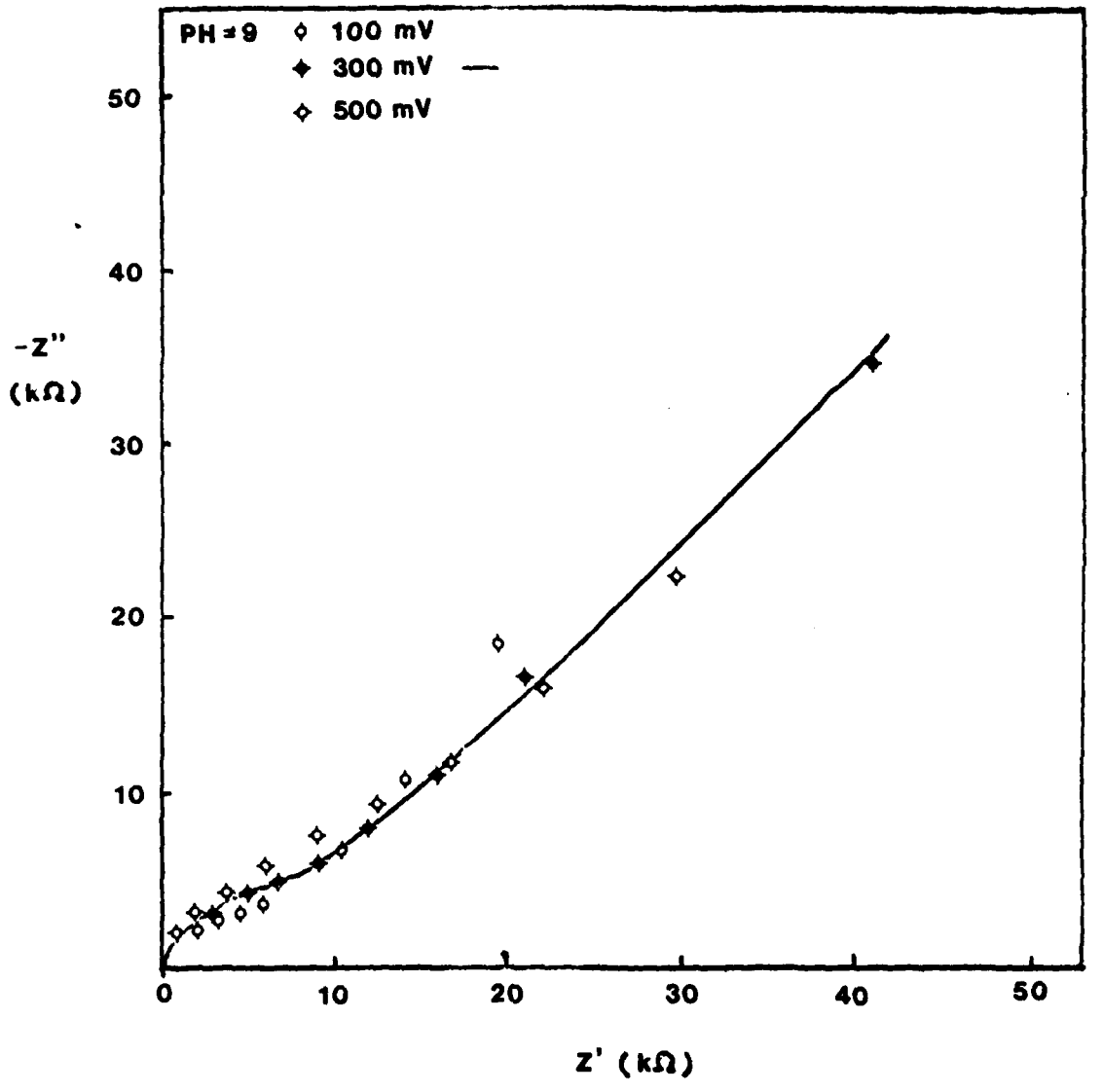

Figure 5. Complex impedance plane for passive nickel (111) in 0.1N phosphate solution (pH = 9).

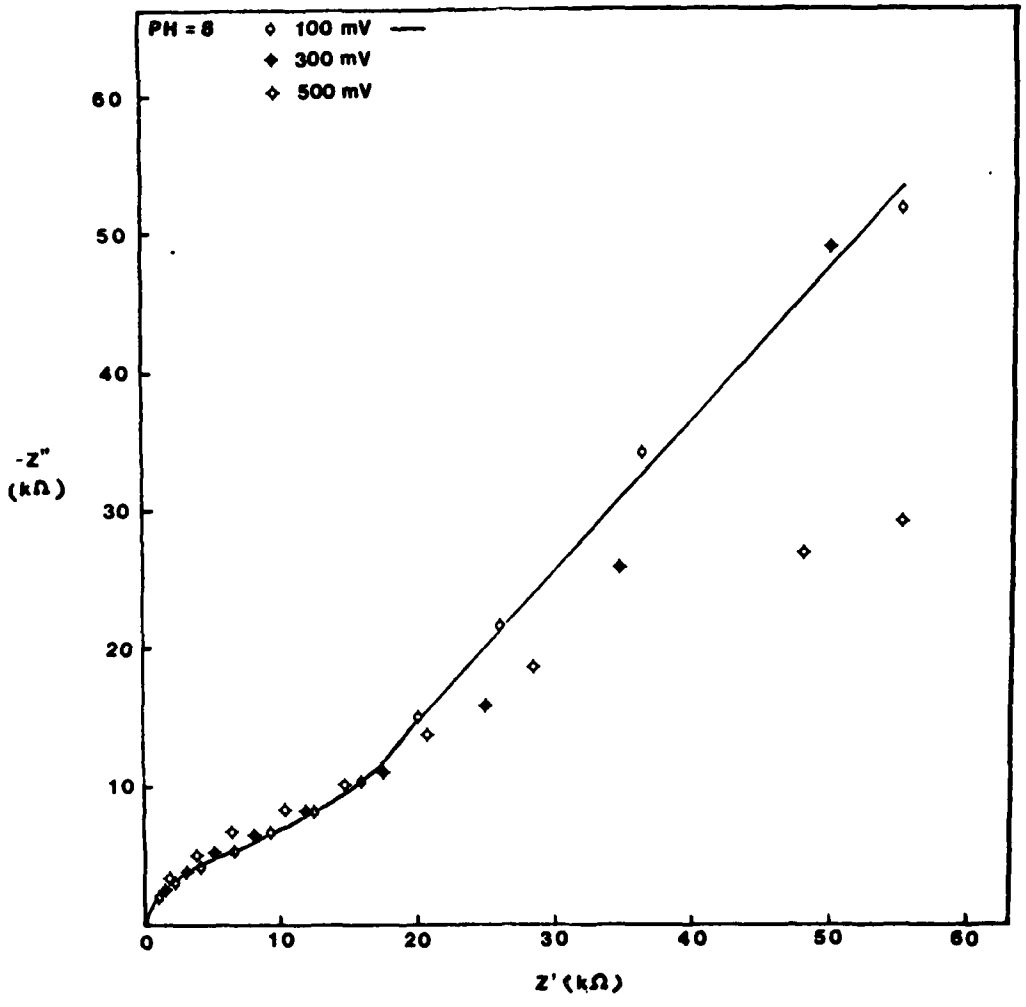

Figure 6. Complex impedance plane for passive nickel (111) in 0.1N phosphate solution (pH = 10).

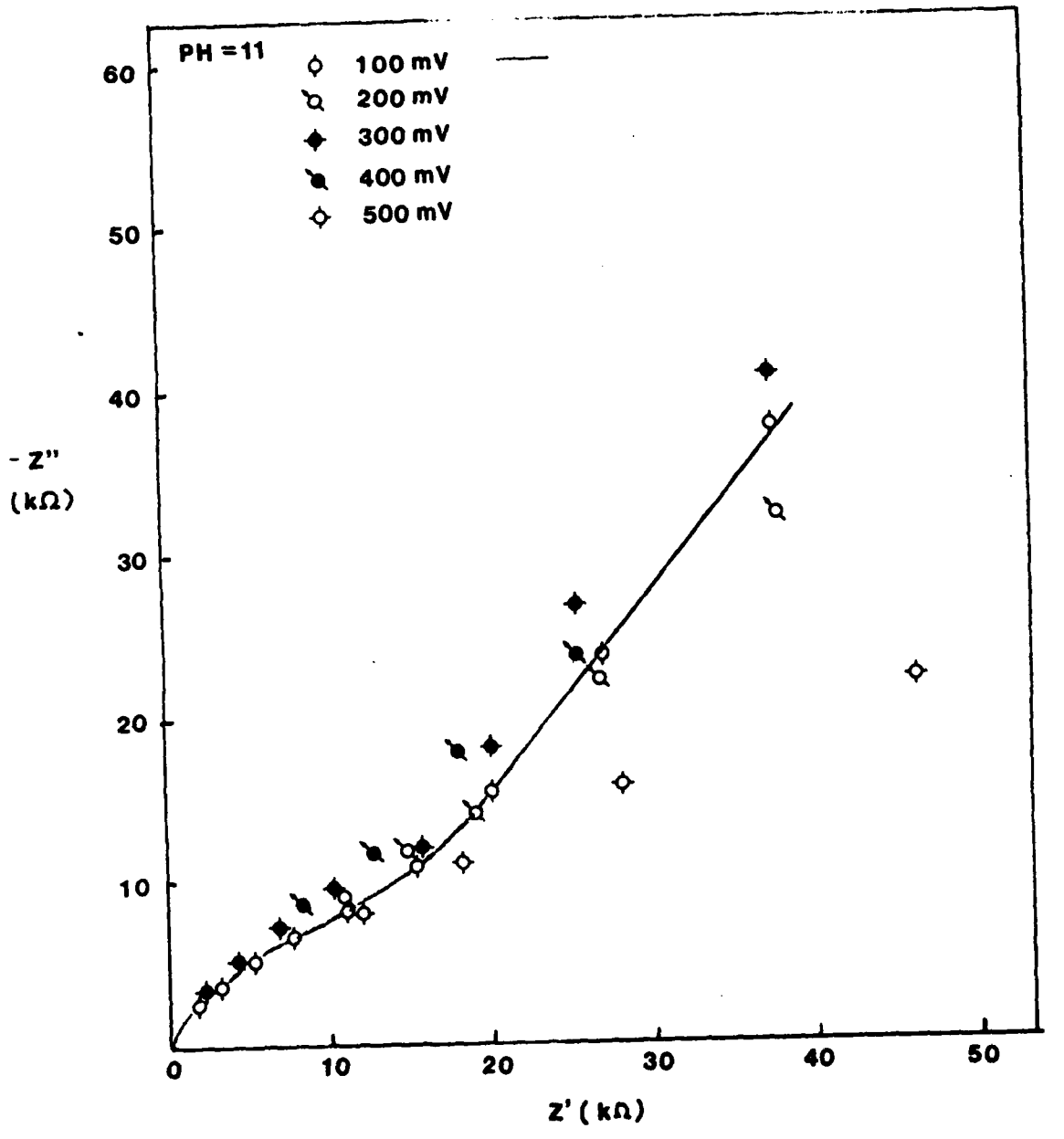

Figure 7. Complex impedance plane for passive nickel (111) in 0.1N phosphate solution (pH = 11).

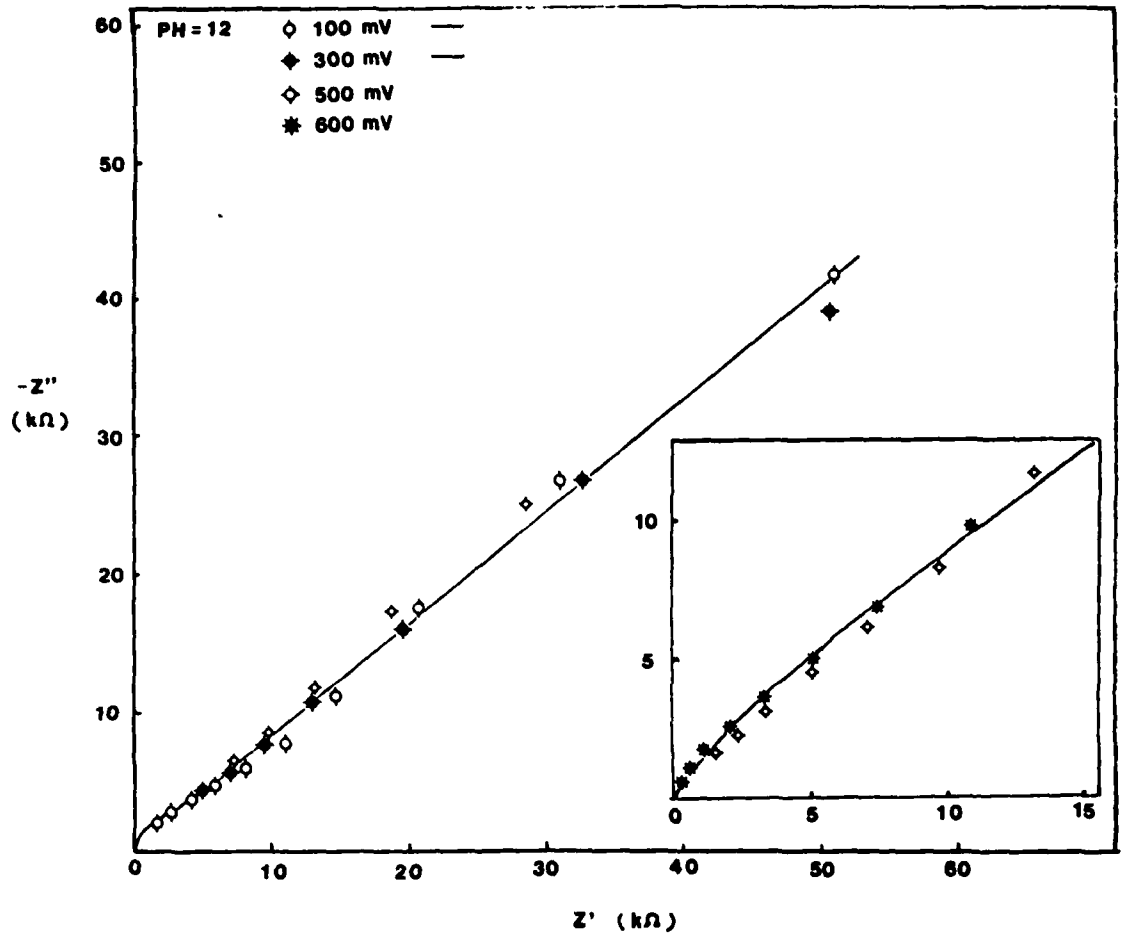

Figure 8. Complex impedance plane for passive nickel (111) in 0.1N phosphate solution (pH = 12).

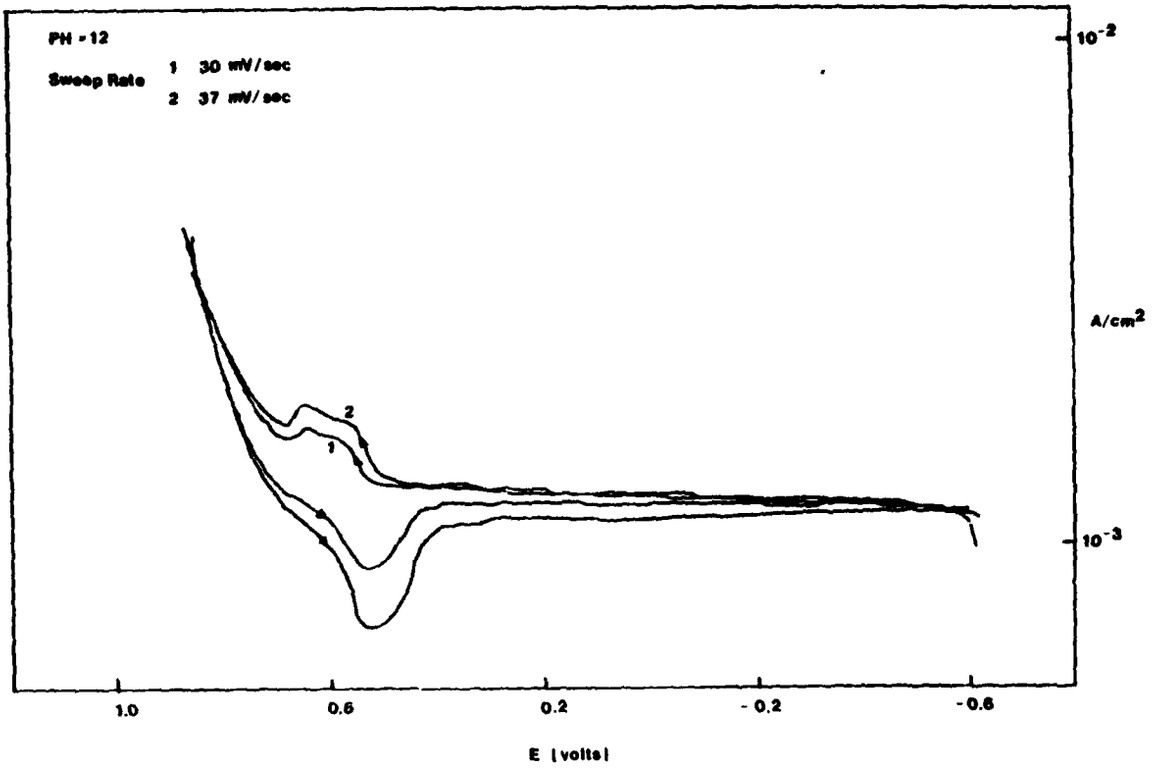

Figure 9. Dependence of current density on potential sweep test for Ni (111) in 0.1N phosphate solution (pH = 12) at two sweep rates.

Secondly, ellipsometric data obtained at $E \geq 600$ mV_{SCE} show a deviation from the theoretical loci for a certain film refractive index (Figure 10) which indicates that the refractive index begins to alter at potentials in the region of +600 mV_{SCE}. Such behavior implies that a transformation of the initial nickel oxidation product commences in this region.

From Figures 11 to 16, the dependence of Z' on $\omega^{-1/2}$ for various values of pH is shown, where δ and σ indicate the film thickness and Warburg coefficient, respectively. A Warburg impedance for a film can be expressed as[3]

$Z_f = (1-j)_{\omega}^{-1/2} \sigma$.

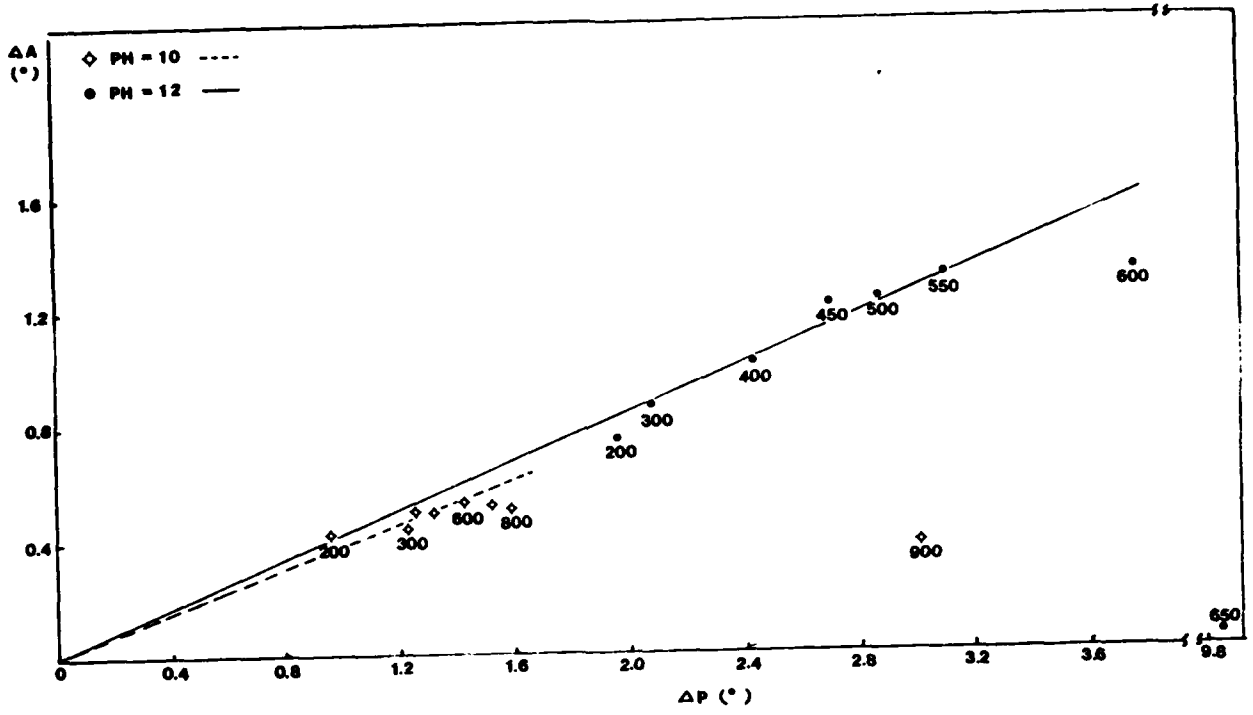

Figure 10. Theoretical loci of ΔA-ΔP for a film refractive index. ◇ and ● indicate experimental data points and the numbers below the points are the applied potentials. Each data point was taken after 15 min anodic polarization except for the first potentials applied which were polarized for 60 min.

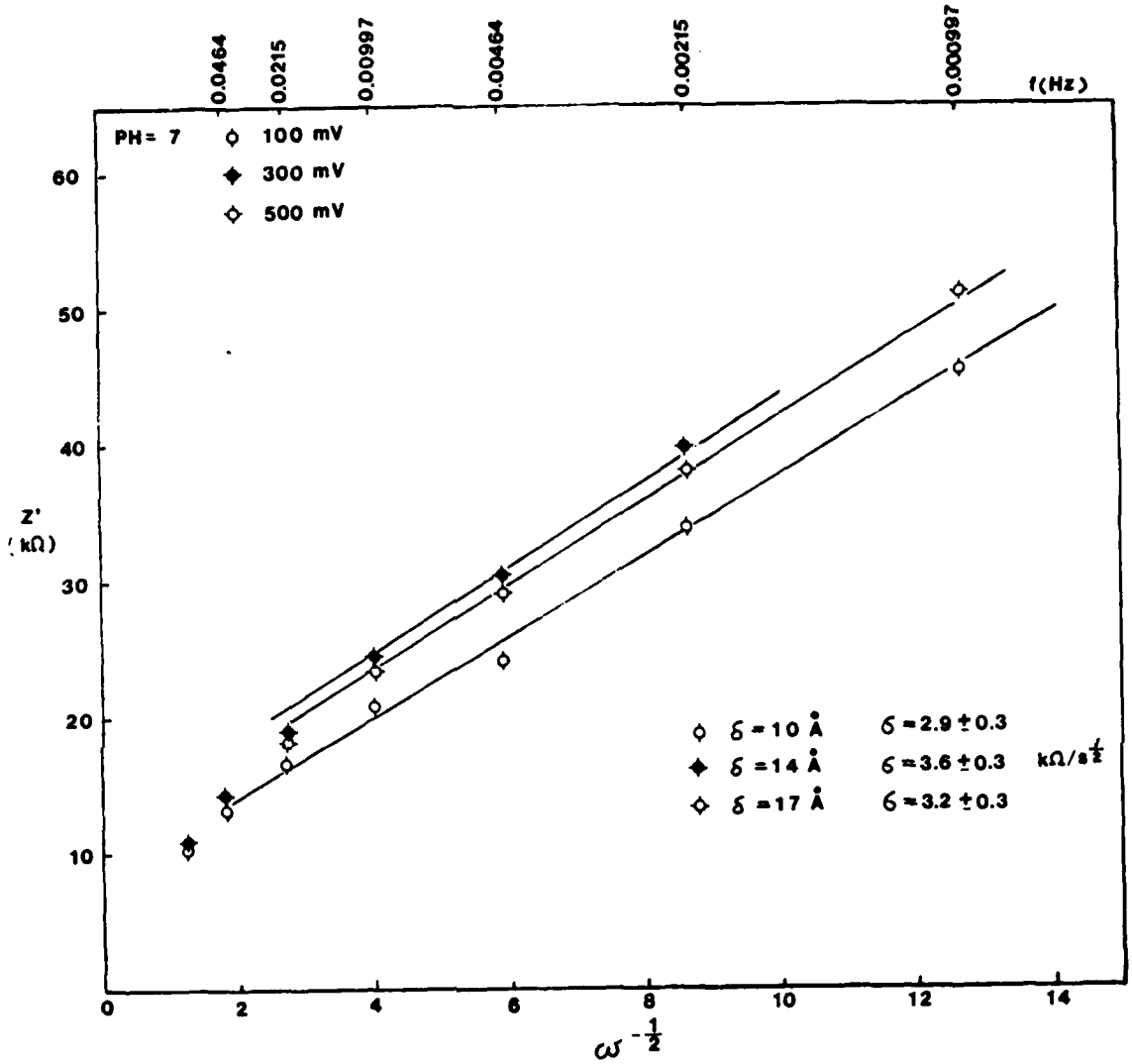

Figure 11. Dependence of Z' on $\omega^{-1/2}$ for Ni (111) passivated in 0.1N phosphate solution (pH = 7).

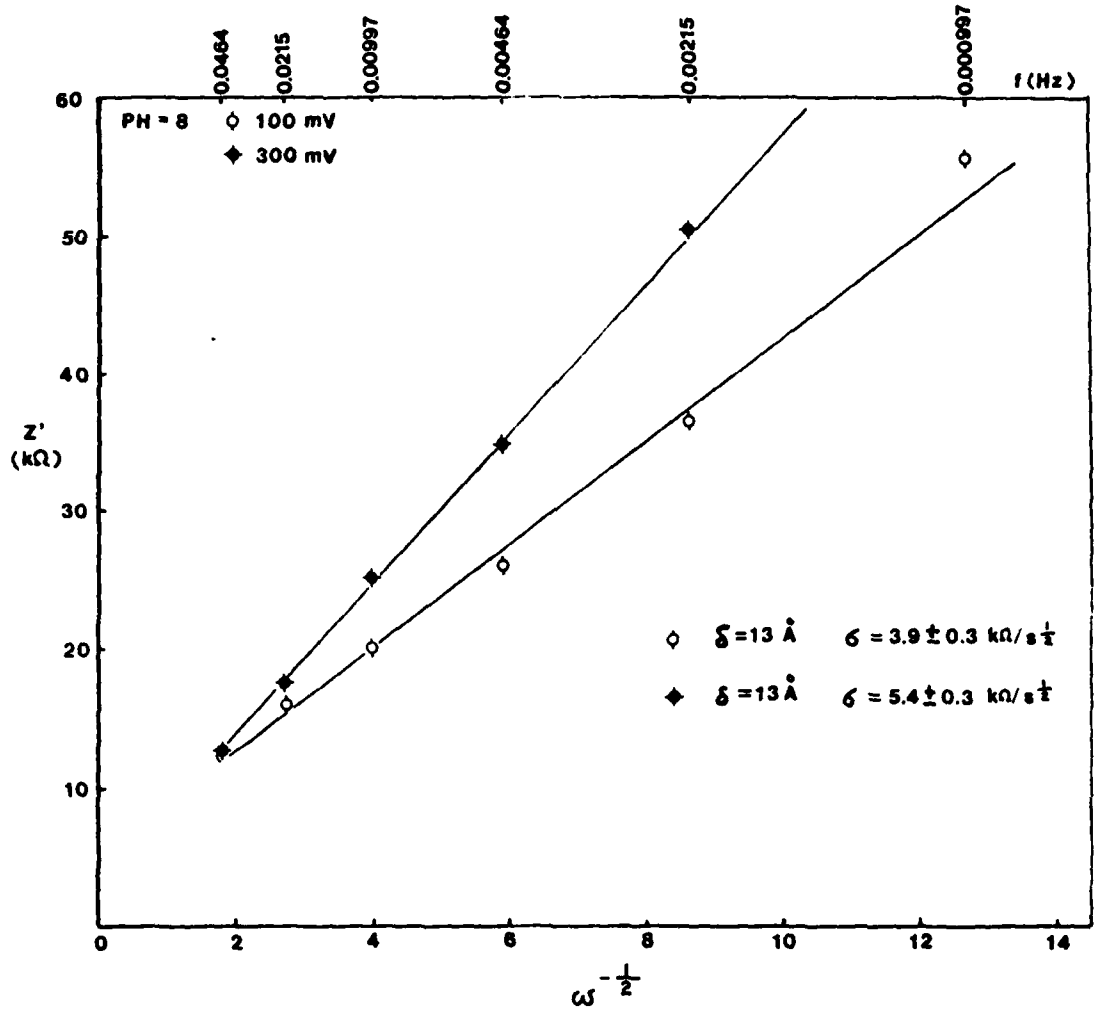

Figure 12. Dependence of Z' on $\omega^{-1/2}$ for Ni (111) passivated in 0.1N phosphate solution (pH = 8).

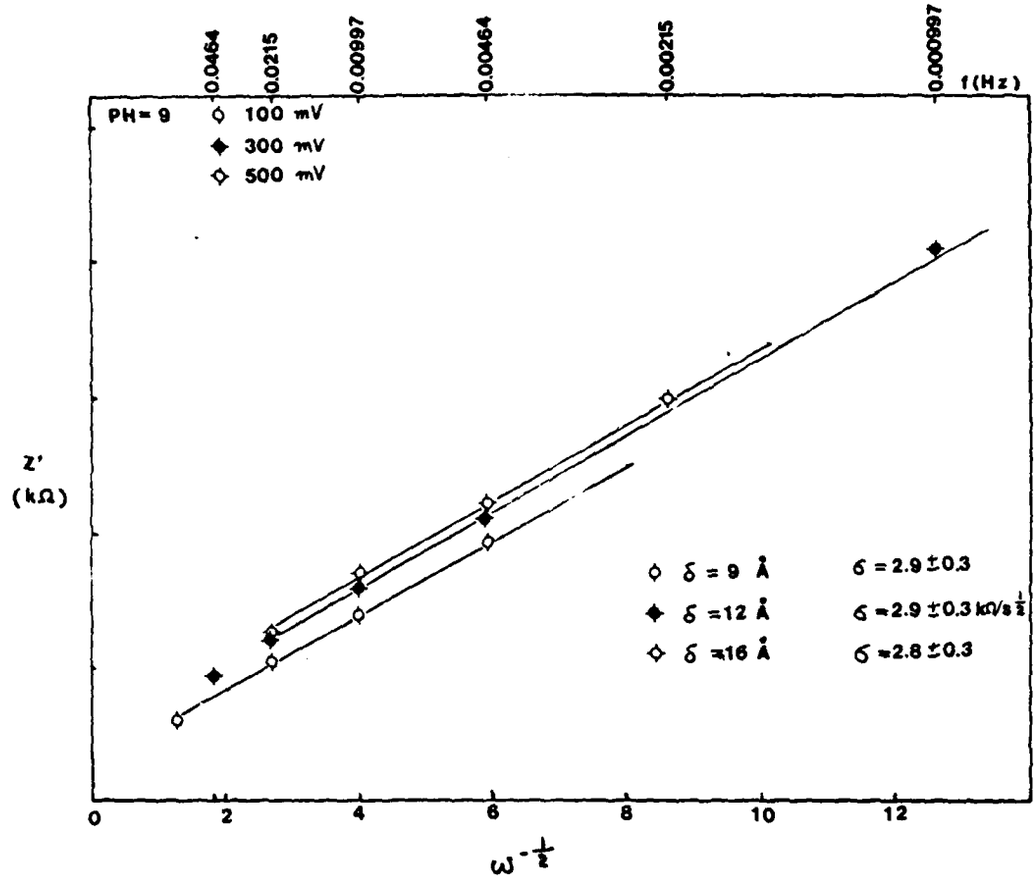

Figure 13. Dependence of Z' on $\omega^{-1/2}$ for Ni (111) passivated in 0.1N phosphate solution (pH = 9).

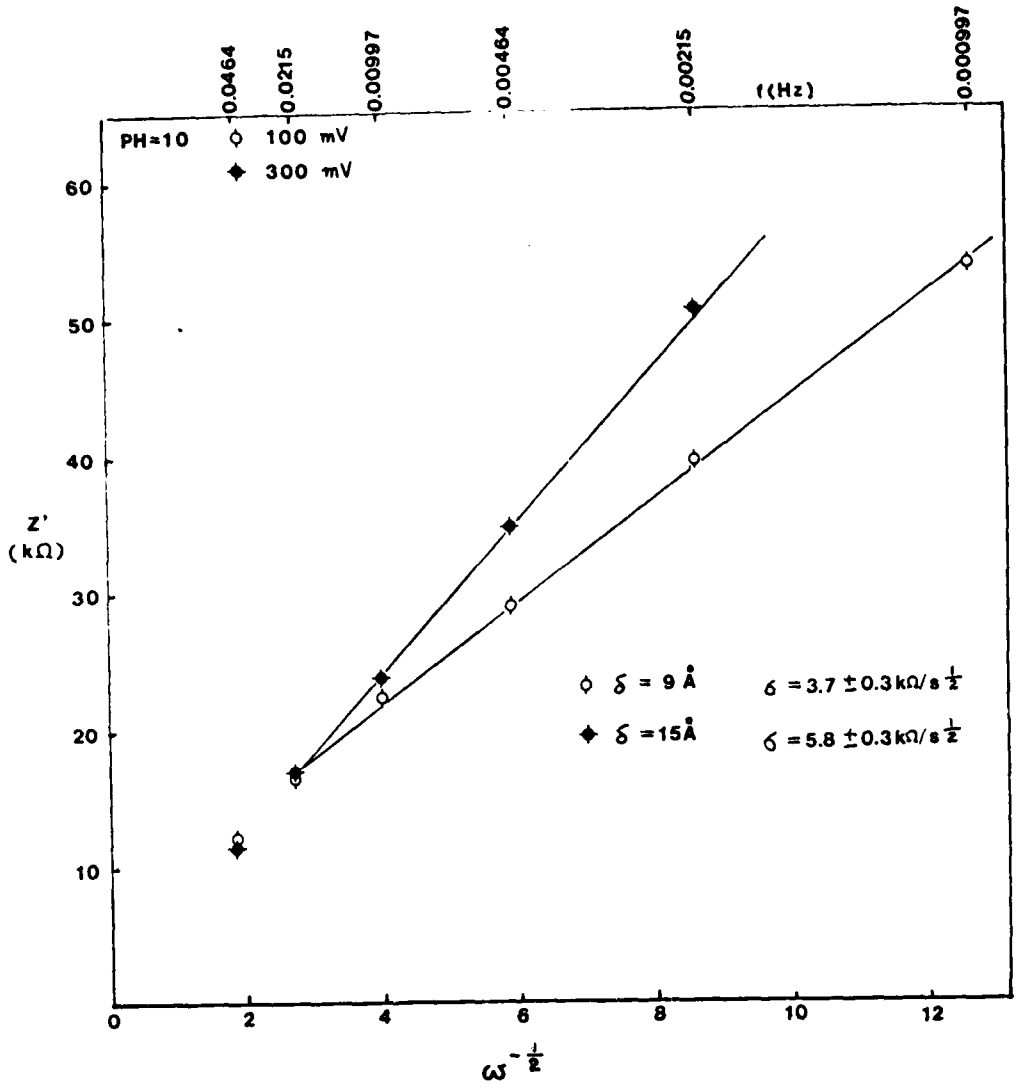

Figure 14. Dependence of Z' on $\omega^{-1/2}$ for Ni (111) passivated in 0.1N phosphate solution (pH = 10).

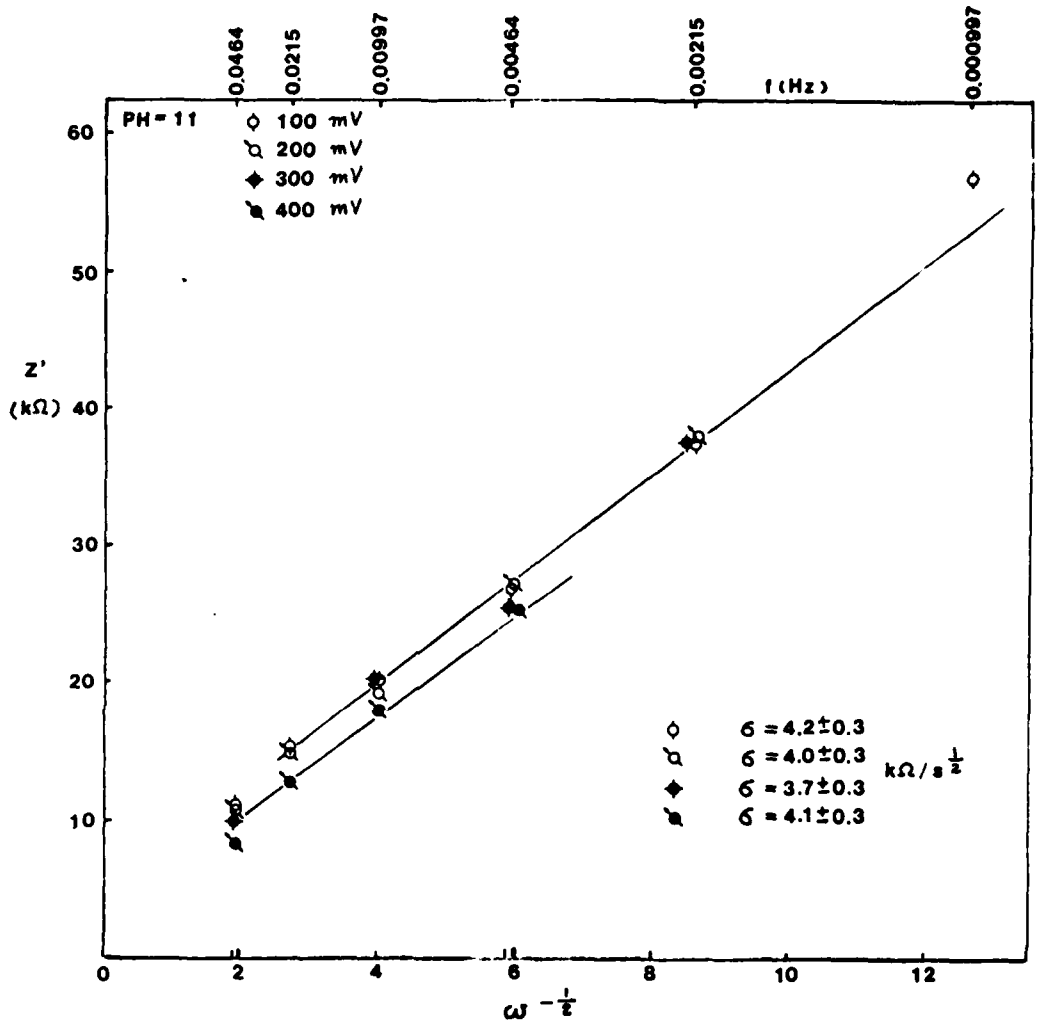

Figure 15. Dependence of Z' on $\omega^{-1/2}$ for Ni (111) passivated in 0.1N phosphate solution (pH = 11).

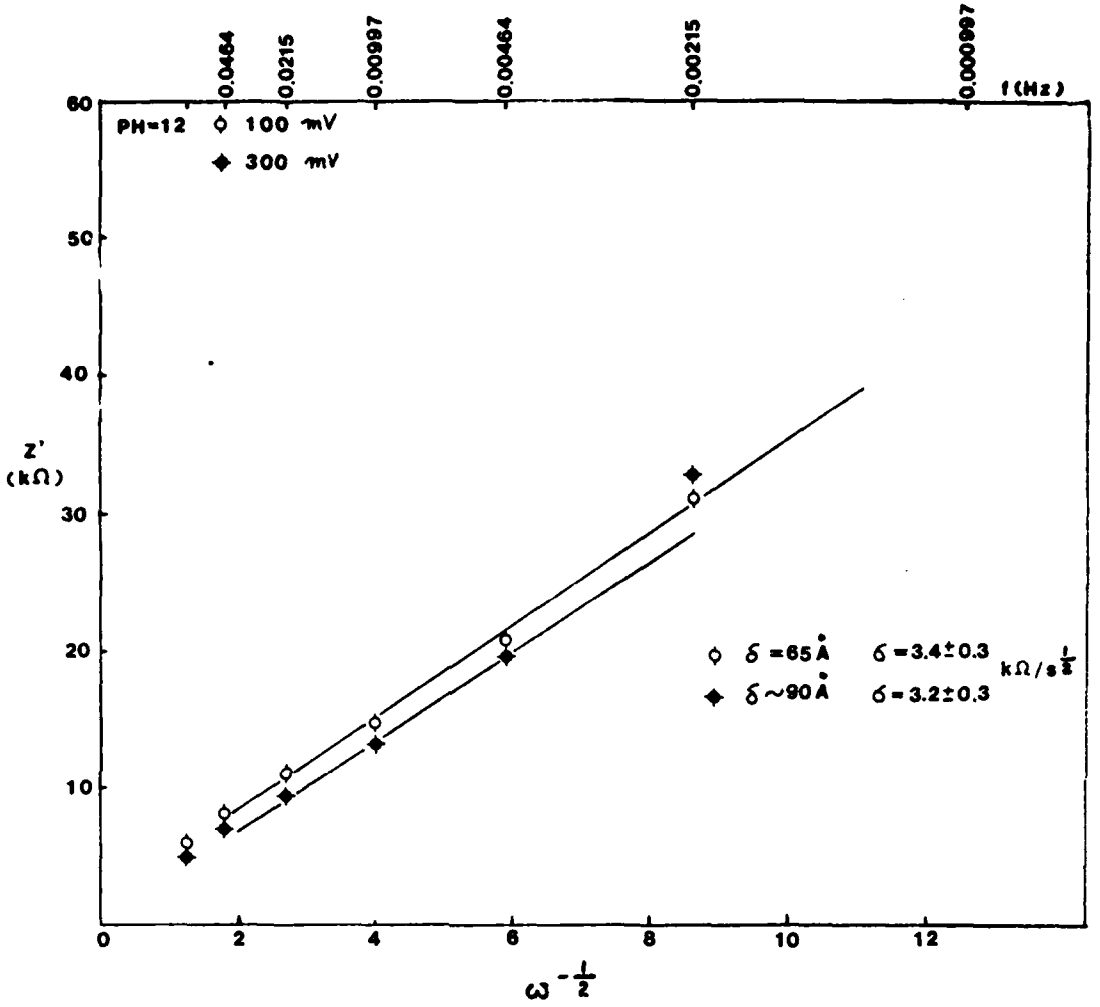

Figure 16. Dependence of Z' on $\omega^{-1/2}$ for Ni (111) passivated in 0.1N phosphate solution (pH = 12).

According to the point defect model[3] which assumes that the film growth rate is controlled by the transport of oxygen anion vacancies under the influence of electric field, σ can be expressed as

$$\sigma = \frac{dZ'}{d\omega^{-1/2}} = \sigma_o = RT/F^2 \sqrt{32D}\left[C_{V_{\ddot{O}}}(m/f)\right]_{dc} (1-\alpha) \qquad (1)$$

where σ_o = the Warburg coefficient associated with oxygen anion vacancies,

$C_{V_{\ddot{O}}}(m/f)$ = the concentration of oxygen anion vacancies at the metal/film interface, and

α = the polarizability of the film/solution interface ($\phi_{f/s} = \alpha \cdot V_{ext} + \phi^\circ$).

Equation (1) can be simplified to give

$$\sigma \cdot I_{dc} = \sqrt{D/2} \times \frac{\varepsilon}{\sqrt{1-\alpha}} \qquad (2)$$

by using the correlation[3] between $\left[C_{V_{\ddot{O}}}(m/f)\right]_{dc}$ and the DC current, I_{dc}. ε represents the electric field strength in the film. An assumption of the point defect model is that the passive film exists on the verge of dielectric breakdown, and therefore ε is a function of the chemical and electrical characteristics of the film.

α is independent of pH and of the identity of the anion in solution[1]. Furthermore, both ε and α have been shown[1] to be potential independent. Therefore, the product of σ and I_{dc} is expected to be a constant. Values of $I_{dc} \cdot \sigma$ were calculated to test this constancy and the results shown in Table 2 indicate considerable promise for the general applicability of equation (2) since $I_{dc} \cdot \sigma$ is indeed constant within experimental error at pH values of 9 and 11. In addition, σ was generally found to be independent of film thickness as seen in Table 2. The lack of a constant $I_{dc} \cdot \sigma$ product at other values of pH is largely due to the difficulty in measuring accurately the small dc currents and particularly in determining a satisfactory steady state.

Table 2

EXPERIMENTAL DC CURRENT (I_{dc}), THICKNESS (δ), AND WARBURG COEFFICIENT (σ) AT VARIOUS POTENTIALS

pH	$E(mV_{SCE})$	$I_{dc}(A)$	$\delta(\AA)$	$(\Omega \cdot sec^{-1/2})$	$I_{dc} \cdot \sigma$ (volt·sec$^{-1/2}$)
7	100	$(0.8\pm0.1)\times10^{-6}$	10	$(2.9\pm0.3)\times10^{3}$	$(2.3\pm0.5)\times10^{-3}$
	300	$(1.1\pm0.1)\times10^{-6}$	14	$(3.6\pm0.3)\times10^{3}$	$(4.0\pm0.7)\times10^{-3}$
	500	$(1.0\pm0.1)\times10^{-6}$	17	$(3.2\pm0.3)\times10^{3}$	$(3.1\pm0.8)\times10^{-3}$
8	100	$(0.3\pm0.1)\times10^{-6}$	13	$(3.9\pm0.3)\times10^{3}$	$(1.2\pm0.5)\times10^{-3}$
	300	$(0.9\pm0.1)\times10^{-6}$	13	$(5.4\pm0.3)\times10^{3}$	$(4.8\pm0.8)\times10^{-3}$
9	100	$(0.7\pm0.1)\times10^{-6}$	9	$(2.9\pm0.3)\times10^{3}$	$(2.0\pm0.5)\times10^{-3}$
	300	$(0.8\pm0.1)\times10^{-6}$	12	$(2.9\pm0.3)\times10^{3}$	$(2.3\pm0.5)\times10^{-3}$
	500	$(0.8\pm0.1)\times10^{-6}$	16	$(2.8\pm0.3)\times10^{3}$	$(2.2\pm0.5)\times10^{-3}$
10	100	$(0.3\pm0.1)\times10^{-6}$	9	$(3.7\pm0.3)\times10^{3}$	$(1.1\pm0.5)\times10^{-3}$
	300	$(0.6\pm0.1)\times10^{-6}$	15	$(5.8\pm0.3)\times10^{3}$	$(3.5\pm0.7)\times10^{-3}$
11	100	$(0.4\pm0.1)\times10^{-6}$	--	$(4.2\pm0.3)\times10^{3}$	$(1.7\pm0.5)\times10^{-3}$
	200	$(0.6\pm0.1)\times10^{-6}$	--	$(4.0\pm0.3)\times10^{3}$	$(2.4\pm0.6)\times10^{-3}$
	300	$(0.5\pm0.1)\times10^{-6}$	--	$(3.7\pm0.3)\times10^{3}$	$(1.9\pm0.5)\times10^{-3}$
	400	$(0.6\pm0.1)\times10^{-6}$	--	$(4.1\pm0.3)\times10^{3}$	$(2.5\pm0.6)\times10^{-3}$
12	100	$(0.4\pm0.1)\times10^{-6}$	65	$(3.4\pm0.3)\times10^{3}$	$(1.4\pm0.5)\times10^{-3}$
	300	$(0.6\pm0.1)\times10^{-6}$	90	$(3.2\pm0.3)\times10^{3}$	$(2.0\pm0.5)\times10^{-3}$

By using equation (2), we are able to determine the diffusion coefficient of oxygen anion vacancies in the nickel passive film since $\epsilon=1.1\times10^{6}$ V/cm, $\alpha=0.878$ (Ref.3) and $\sigma \cdot I_{dc} = 2.1\times10^{-3} V sec^{-1/2}$ for a nickel single crystal (111) in 0.1N phosphate solution (pH=9). Therefore, $D_{(single)} \cong 1.0\times10^{-19}$ cm^2/sec. This value is 100 times larger than that obtained for polycrystalline Ni ($D \cong 1.3\times10^{-21} cm^2/s$)[3] under the same experimental conditions. If the difference in diffusivities of a single crystal and a polycrystal were caused by the grain boundaries only, $D_{(poly)}$ should be larger than $D_{(single)}$ since the grain boundaries in polycrystalline Ni serve as high-diffusivity paths. However,

$I_{dc(poly)}$ was reported[3] as $1x10^{-8}$A which is an order of magnitude smaller than the values for single crystal Ni. It is clear from equation (2) that this factor alone would account for the above anomaly in the diffusivities.

In Figures 17-22, theoretical loci of Δ vs ψ are shown for various values of pH. The numbers above the loci indicate theoretically calculated film thicknesses and the numbers below the loci indicate the applied potentials. For pH=11 and pH=12, the refractive indices differ from those obtained at other values of pH. This difference could be due to either incorrect theoretical loci selection or experimental error in the ellipsometric measruements.

CONCLUSIONS

This study leads to the following conclusions:

1. The structure of the passive film grown at higher passivation potentials (more positive than +500 mV_{SCE}) is different from that grown at lower potentials. In other words, the passive region is separated into two parts: a $Ni(OH)_2$ film grows at lower potentials, and NiOOH forms at higher potentials.
2. For the potentials at which $Ni(OH)_2$ grows, the constancy of $I_{dc}x\sigma$ is experimentally demonstrated for 0.1N phosphate solutions at various values of pH.
3. The thckness of "steady state" passive films is independent of the Warburg coefficient.
4. Significant difference in diffusivity was found between a single crystal and a polycrystal Ni, i.e., $D_{(single)} \cong 10^{-19}$ cm^2/sec and $D_{(poly)} \cong 10^{-21}$ cm^2/sec.

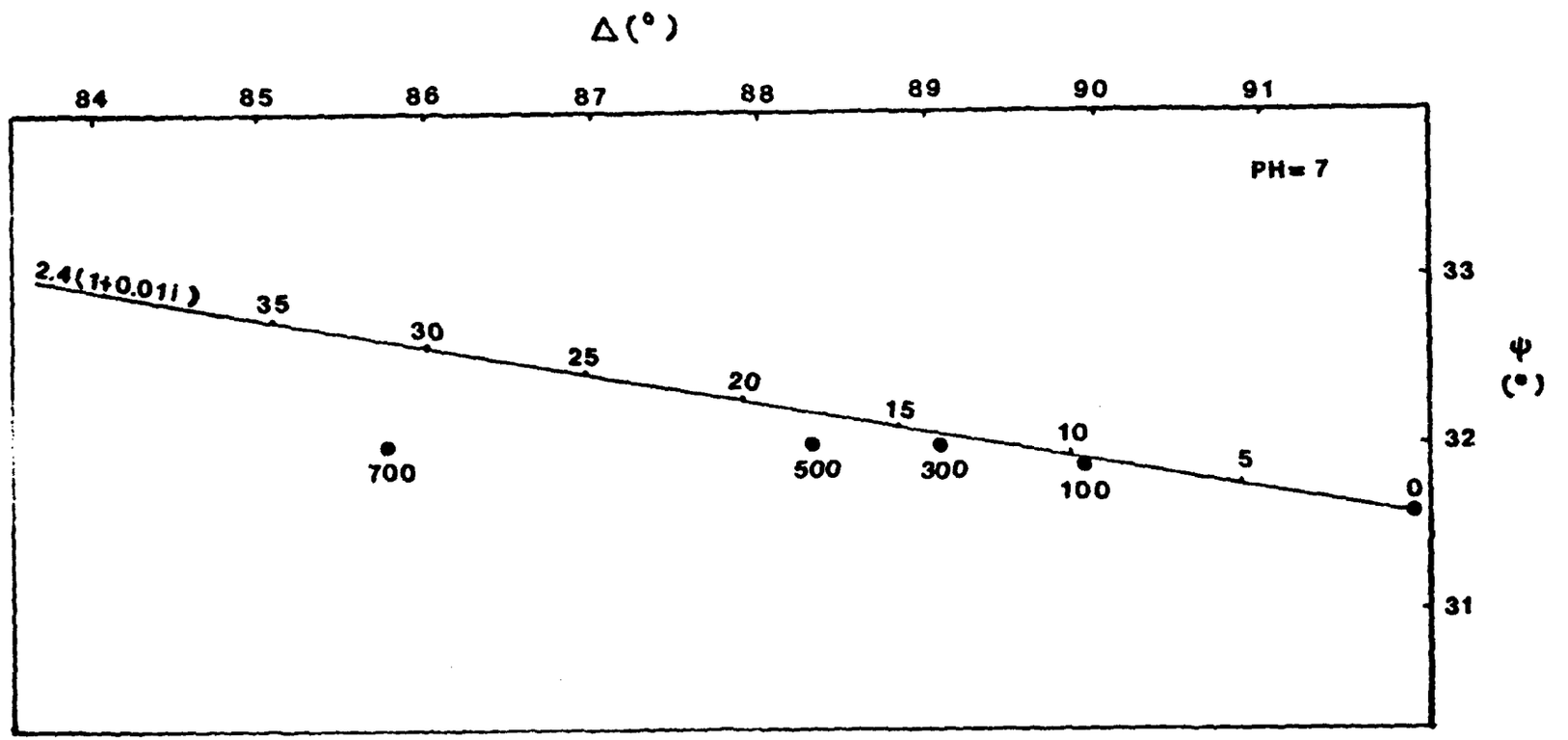

Figure 17. Theoretical locus of ψ-Δ for the passive film on Ni (111) in 0.1N phosphate solution (pH = 7). The numbers above the locus are film thickness in Å and the numbers below the locus are applied potentials.

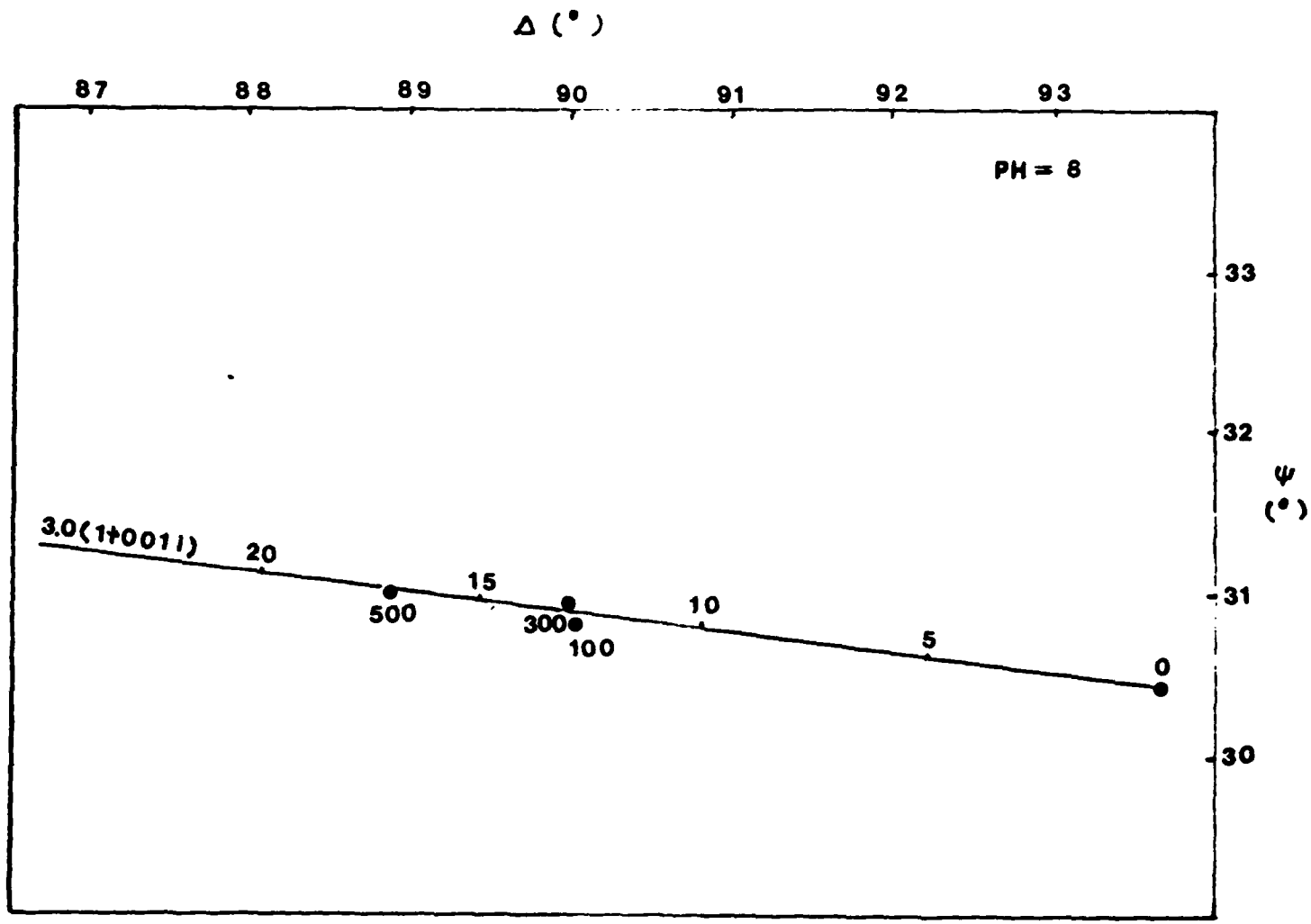

Figure 18. Theoretical locus of ψ-Δ for the passive film on Ni (111) in 0.1N phosphate solution (pH = 8).

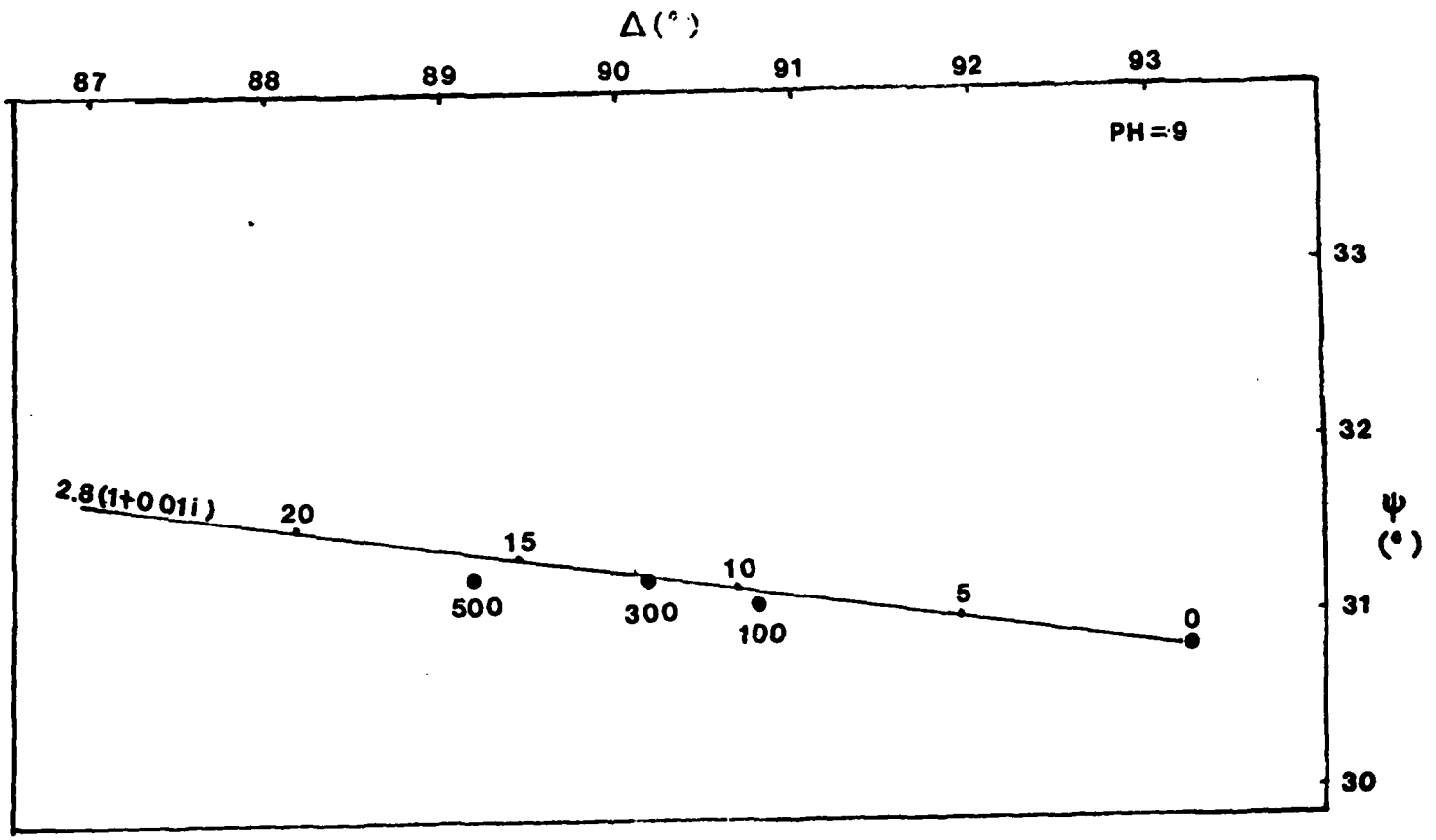

Figure 19. Theoretical locus of ψ-Δ for the passive film on Ni (111) in 0.1N phosphate solution (pH = 9).

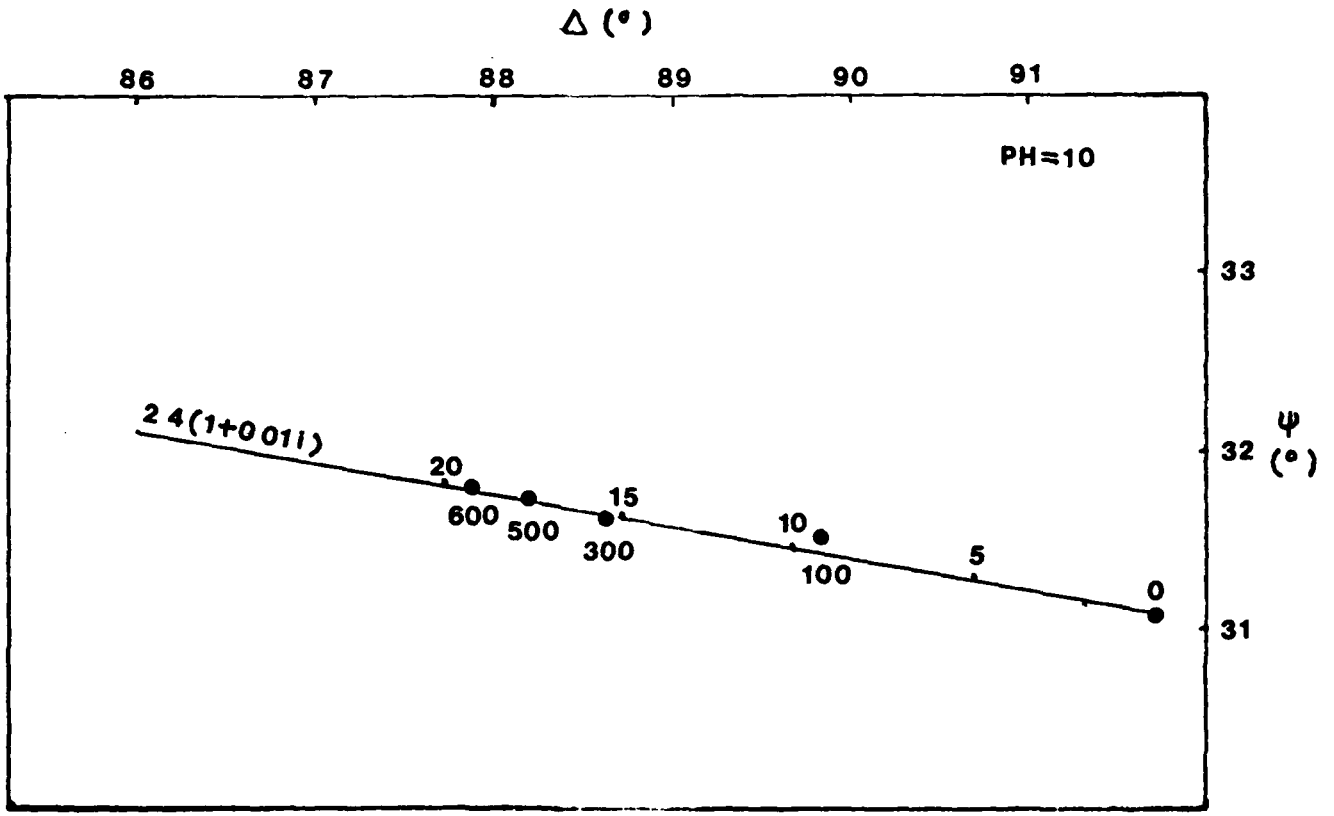

Figure 20. Theoretical locus of ψ-Δ for the passive film on Ni (111) in 0.1N phosphate solution (pH = 10).

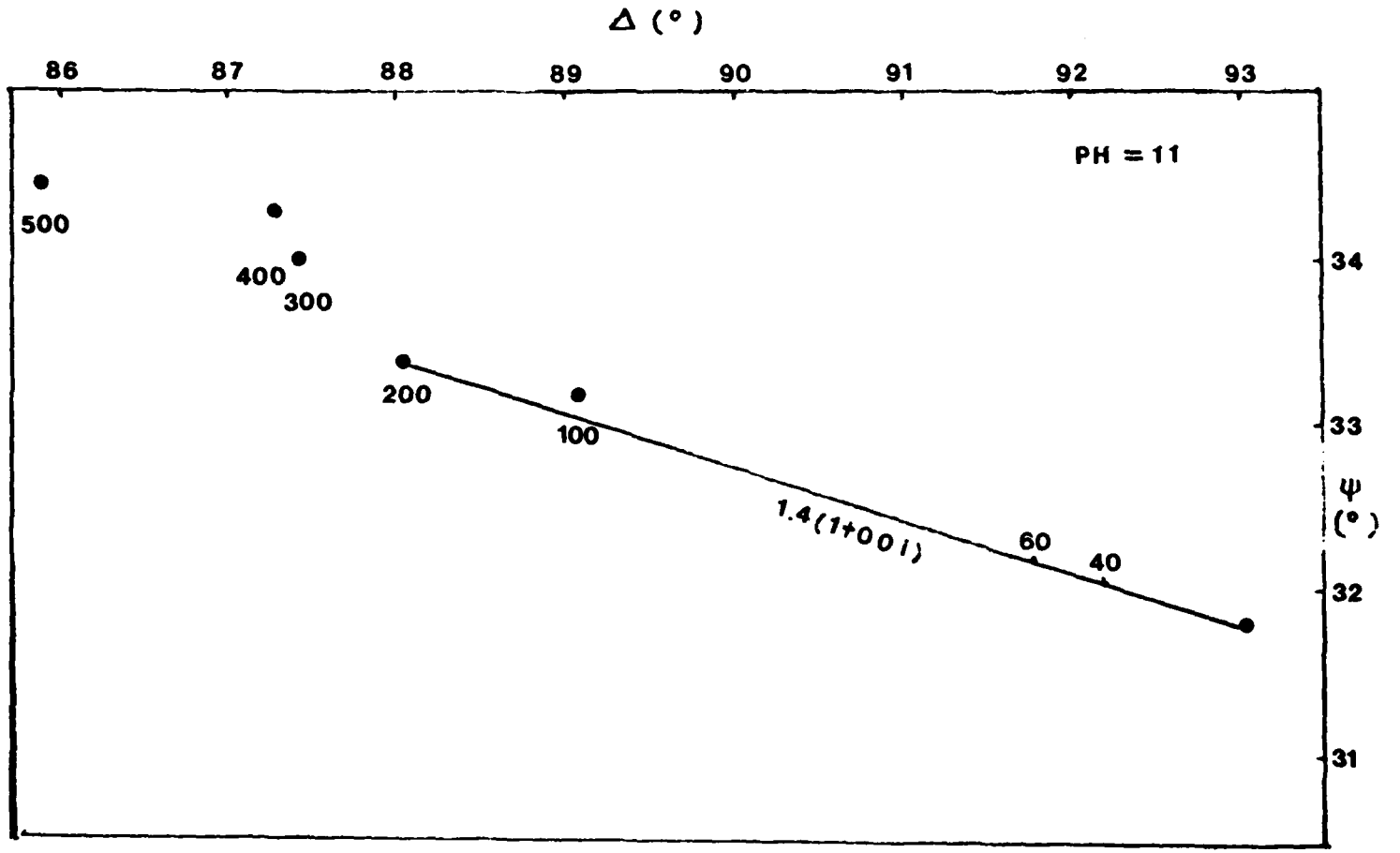

Figure 21. Theoretical locus of ψ-Δ for the passive film on Ni (111) in 0.1N phosphate solution (pH = 11).

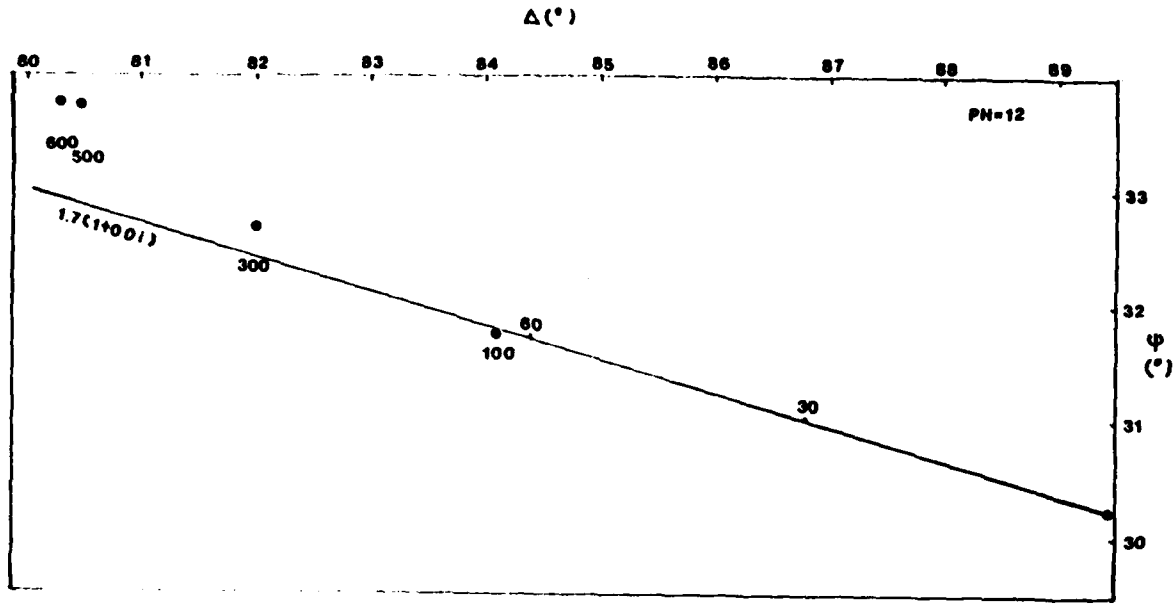

Figure 22. Theoretical locus of ψ-Δ for the passive film on Ni (111) in 0.1N phosphate solution (pH = 12).

REFERENCES

1. C.Y. Chao, L.F. Lin and D.D. Macdonald, J. Electrochem. Soc., 128, 1187 (1981).

2. D.C. Silverman, Corrosion, 37, 546 (1981).

3. C.Y. Chao, L.F. Lin and D.D. Macdonald, J. Electrochem. Soc., 129, 1874 (1982).

Task 7

FILM BREAKDOWN STUDIES

Kaun-Shaur Lei, Bruce Pound, and Digby D. Macdonald

INTRODUCTION

The objective of this film breakdown study is to obtain experimental data on well-defined metal surfaces in order to evaluate and, if necessary, improve the point-defect model[1] for pitting corrosion. The pitting behavior of certain metals is determined by both the "intensive variables" (e.g., crystallographic orientation, grain boundaries, solute atoms, etc.) and the "extensive variables" (e.g., the nature of the electrolyte, the Cl^- anion concentration, film thickness, etc.). This study uses electrochemical and metallurgical techniques to investigate the film breakdown behavior on pure metal (Ni, Fe) single crystals and polycrystals, alloy (Fe-Ni, Fe-Ni-Cr) single crystals, amorphous pure metals and alloys, and finally polycrystalline alloys. At the conclusion of this study, it is expected that extensions to the point defect model will greatly enhance its capability to interpret experimental data.

Currently, this study is focused on the measurement of film breakdown potentials (V_b) on a pure Ni single crystal (100) surface as a function of anodic potential sweep rate, passivation time, and chloride anion concentration.

A major problem that occurred in the first period of this work lay in obtaining a satisfactory sample surface. Surface defects that remained after

polishing led to inconsistent results in film-breakdown experiments. As a result, considerable attention has since been given to developing a polishing procedure which will give a reproducible surface.

EXPERIMENTAL DETAILS

The experimental technique uses a Wenking Model 66TS10 electronic potentiostat as the primary potential control, and a Princeton Applied Research (PAR) Model 175 universal programmer as a wave form generator. A PAR 379 digital coulometer is employed to measure the amount of charge and current passed. A Hewlett-Packard 7047A X-Y recorder and an Esterline-Angus Model L1102S strip-chart recorder record the current/potential and charge/time curves, respectively. Figure 1 shows the experimental set-up.

The first step of this experiment is to polish the sample. After polishing, the Ni electrode is immersed in deaerated borate buffer solution (0.15N H_3BO_3/0.15N $Na_2B_4O_7$/x mole/liter [Cl^-], x=0.01 to 0.1, pH=8.9) and cathodically reduced at -900 mV (vs SCE) for 10 min. A multilayer of oxide film is grown by stepping the potential to a value (-100mV) in the passive region. A potential sweep in the anodic direction is started after a time (t_p) at -100 mV, and the sweep direction is reversed shortly after pitting occurs. The potential-time profile is shown in Figure 2. The film breakdown potential (V_b) is found from the I-V curve obtained using the X-Y recorder.

During this period of the study, most of the effort has been devoted to the sample polishing procedure. In order to reveal the pitting characteristics of the pure Ni single crystal, a reproducible, defect-free surface must be obtained by polishing before each pitting experiment. A mechanically polished surface gives inconsistant results because the surface deformation

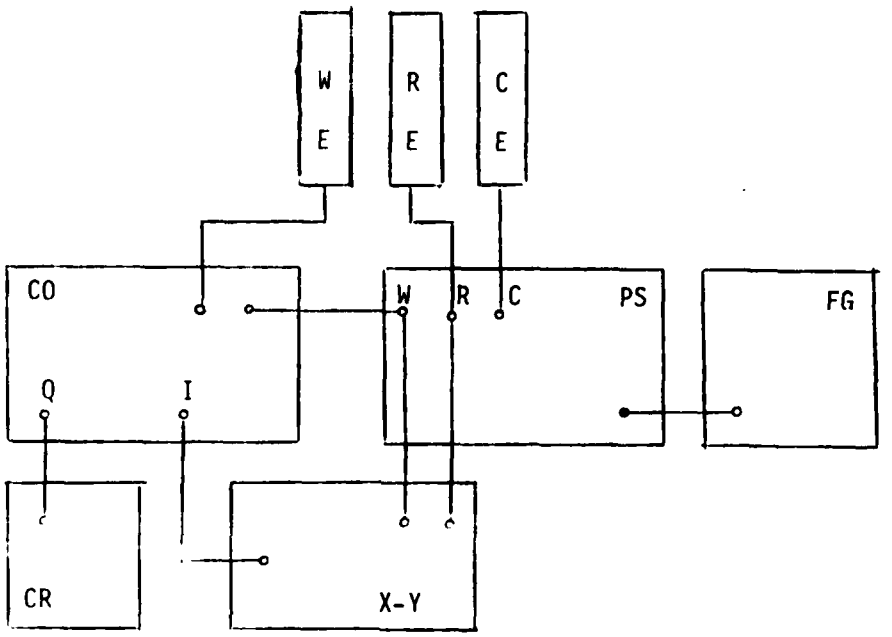

Figure 1. Film breakdown experimental setup.
WE - Working electrode CO - Coulometer
CE - Counter electrode FG - Function Generator
RE - Reference electrode PS - Potentiostat
CR - Chart recorder X-Y - X-Y recorder

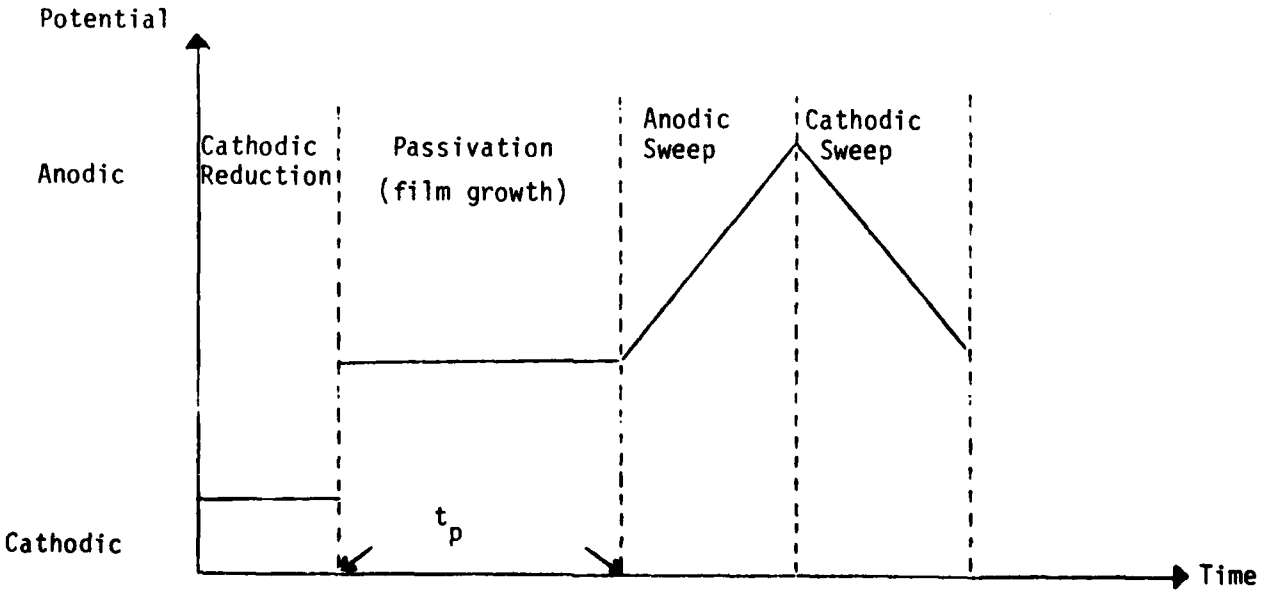

Figure 2. Potential-time profile in film breakdown studies.

layer, scratches and holes produced by polishing provide heterogeneous pit nucleation sites. Several combinations of mechanical, chemical, and electrolytic polishing procedures have been tried. The best result is obtained by first mechanically polishing with emery paper (320-600 grit), diamond paste, and alumina powder (down to 0.05 μm), then electro-polishing in 57% (by volume) H_2SO_4 at about 1.4 V for 15 seconds to remove mechanical damage. Although an absolutely defect-free surface is too difficult to produce, a satisfactory surface condition is obtained with the above procedure. Optical micrographs of mechanically-polished and mechanically/electrolytically-polished surfaces are shown in Figure 3. The difference in the polarization behavior between these two polishing procedures can be seen in Figure 4.

Crevice corrosion, which generally occurs before pitting corrosion, was observed to occur in initial experiments in this study. This problem was overcome by applying microstop* to the sample-tube crevice and adding a teflon shield with a small opening above the sample. The use of a screen which is similar to the shield has been found by Smialowska and Mankowski[2] to be effective in avoiding crevice corrosion. The shield design is shown in Figure 5. The microstop covers the major tube-sample crevice, while the shield reduces the current density at the microscopic microstop-sample crevice. Consequently, pitting does not occur at either place. The shield is kept at about 3mm away from the sample surface so that the shield-sample gap is large enough not to be considered as a crevice. This shield design also allows unrestricted access for the electrolyte, and therefore, the compositon of the solution at the sample surface is the same as that of the bulk solution during the experiment.

*Microstop is a lacquer manufactured by Michigan Chrome and Chemical Company.

(A)

(B)

Figure 3. Optical micrograph of polycrystalline Ni by (A) mechanical polishing (50X) and (B) mechanical plus electrolitical polishing (100X).

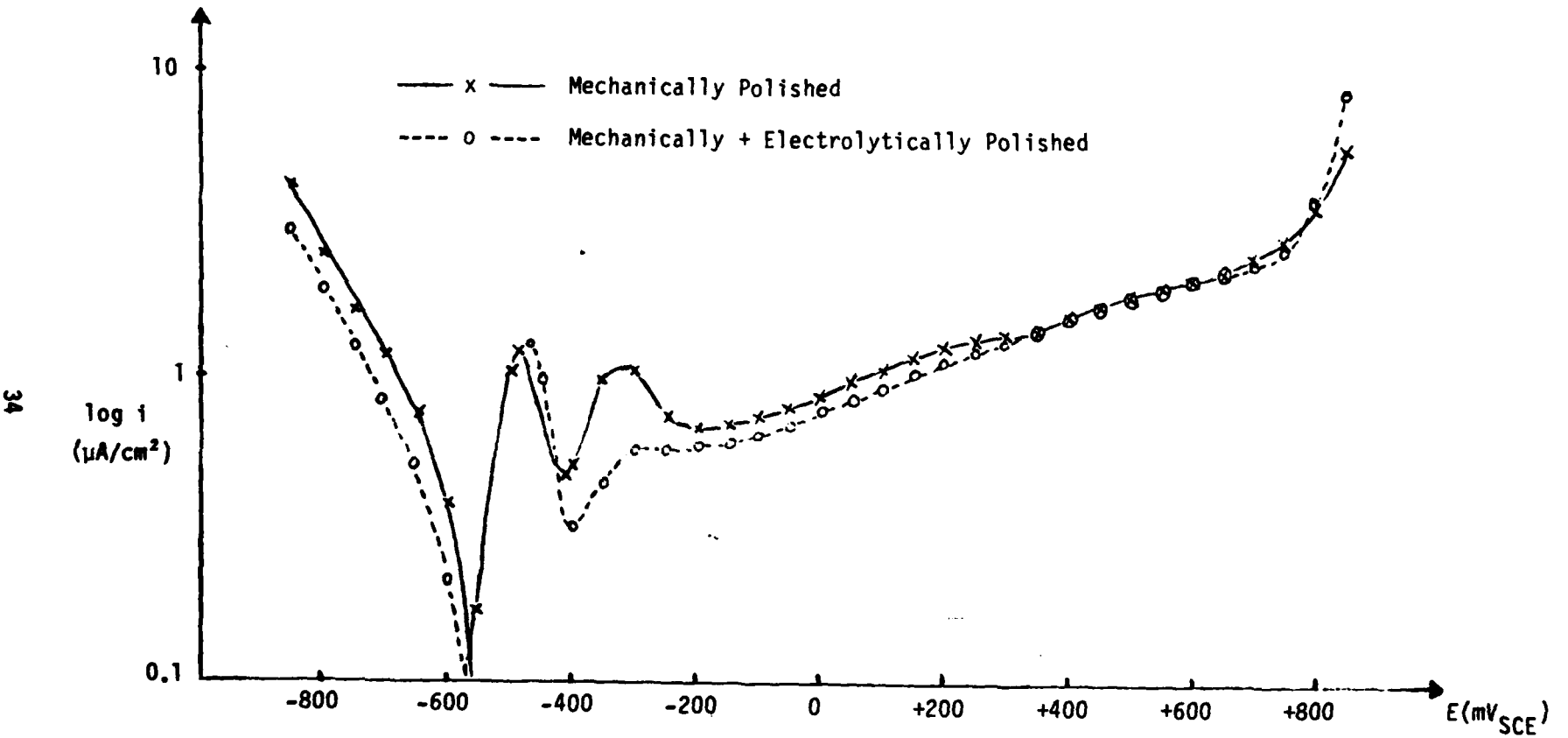

Figure 4. Polarization curves of pure Ni (100) by mechanical polishing and by mechanical plus electrolytical polishing.

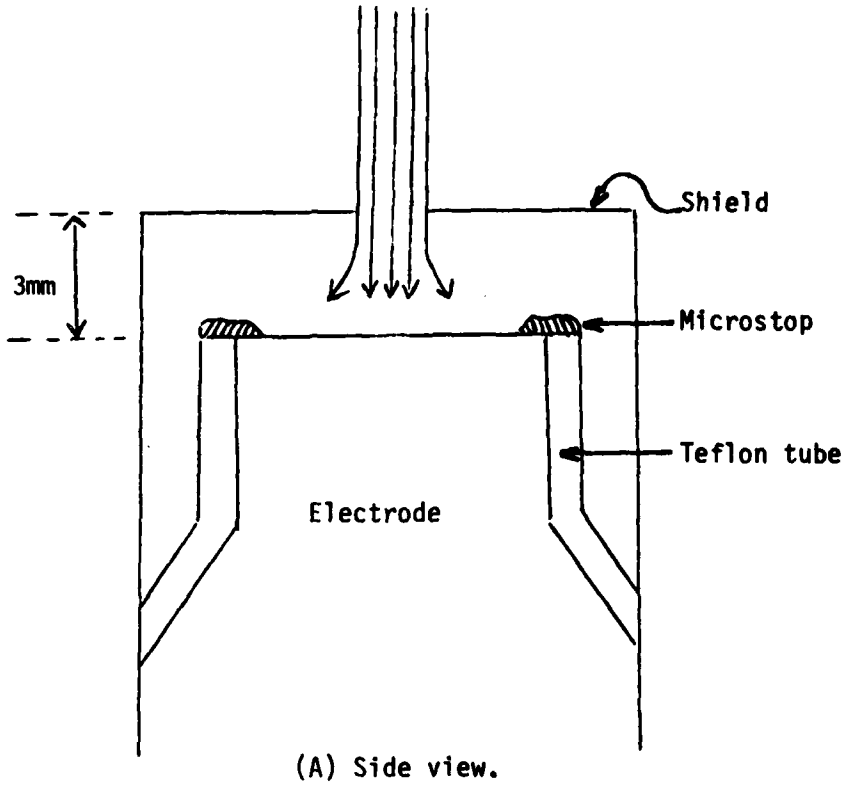

(A) Side view.

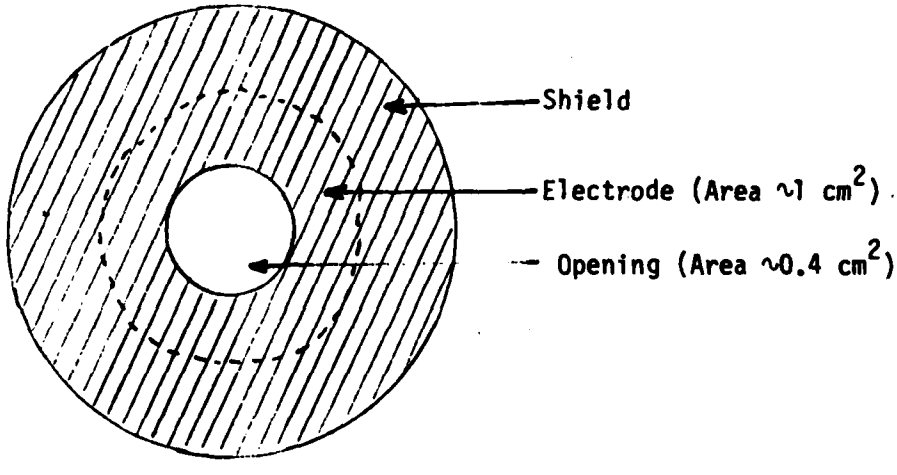

(B) Top view.

Figure 5. Shield design to avoid crevice corrosion.

RESULTS AND DISCUSSION

Several film breakdown experiments have been performed on an electropolished Ni (100) sample at different chloride concentration, passivation times (t_p), and anodic sweep rates (∇=dv/dt). Figure 6 shows a typical I-V curve for a film breakdown experiment. The results are listed in Table 1. Qualitatively, the results show that the breakdown potential is increased as the sweep rate increases, the passivation time increases, or the chloride concentration decreases. At this point, insufficient data preclude a quantitative analysis of the results.

Table 1

FILM BREAKDOWN POTENTIAL (V_b) AT DIFFERENT PASSIVATION TIMES (t_p), CHLORIDE ION CONCENTRATION (Cl^-), AND SWEEP RATES (∇).

$[Cl^-]$ (moles/ℓ)	t_p (min)	∇ (mV/sec)	V_b (mV_{SCE})
0.1	5	20	770
0.1	5	10	465
0.1	20	10	760
0.01	5	10	650

SUMMARY

During this reporting period, the main progress was in successfully developing a sample polishing procedure and shield design. The combination of mechanical and electrolytic polishing creates a reproducible, nearly defect-free surface which is an essential requirement for revealing film breakdown behavior. The shield design ensures that pitting corrosion without crevice corrosion occurs. Some film breakdown potentials (V_b) were measured, but analysis of the data cannot be performed as yet.

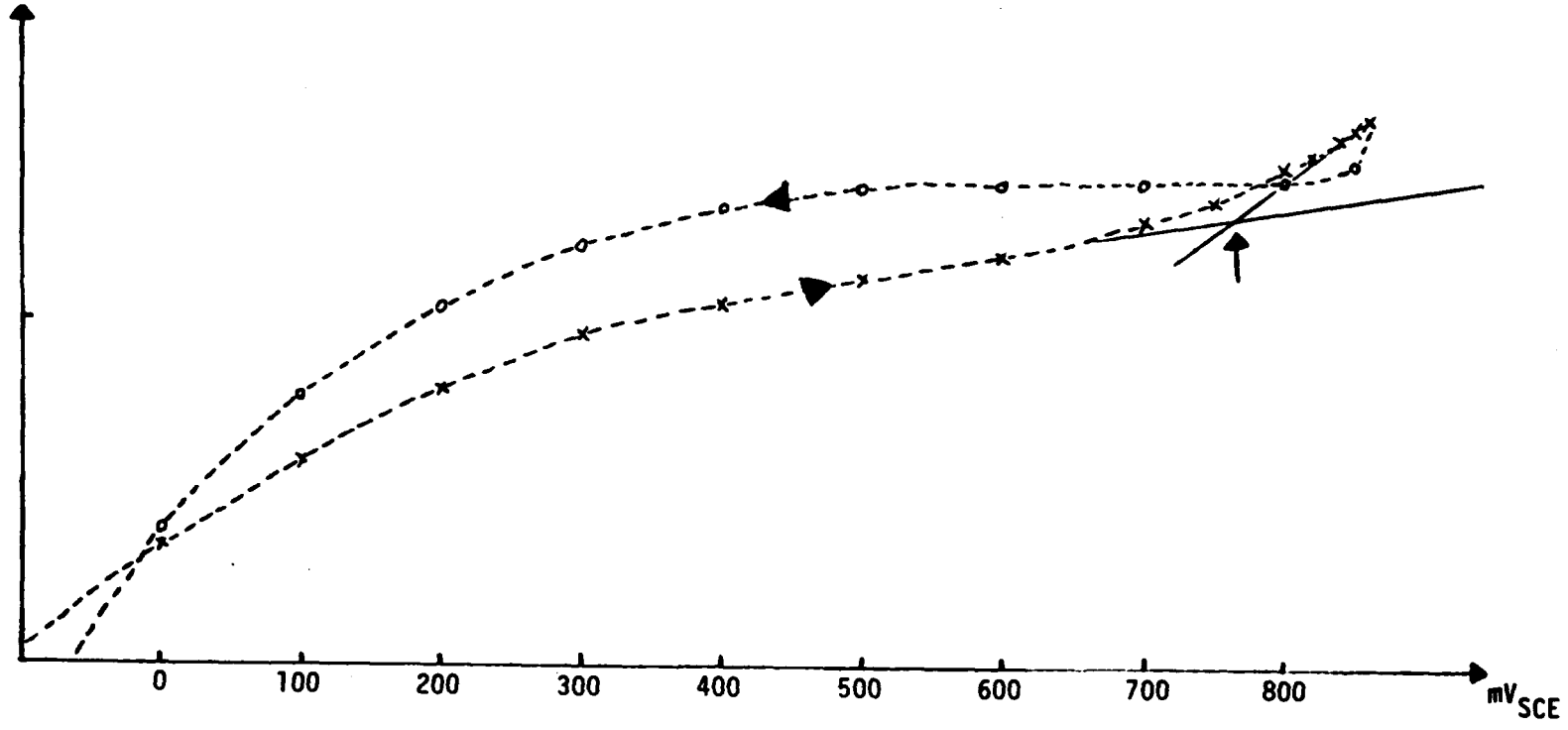

Figure 6. I-V curve of Ni (100) in film breakdown studies.

FUTURE WORK

Work for the next period will involve the following:

1. Measure the breakdown potentials on pure Ni (100) surfaces for different sweep rates and obtain the critical breakdown potential (V_c) by extrapolating V_b to zero sweep rate.
2. Measure critical breakdown potentials (V_c) for different chloride ion concentrations and film thicknesses so as to evaluate the first prediction of the point defect model[3].
3. Measure the incubation time at different breakdown overpotentials (ΔV).

REFERENCES

1. C.Y. Chao, L.F. Lin, and D.D. Macdonald, J. Electrochem. Soc., 128, 1187 (1981).
2. S. Smilalowska and J. Mankowski, Corr. Sci., 22, 1105(1982).
3. R.Y. Liang, K.S. Lei, B.G. Pound, and D.D. Macdonald, Non-Technical Report to ONR, FCC4445-1, Sept. 1, 1982.